Journal of Marine Research, 66, 219–254, 2008

Worms as wedges: Effects of sediment mechanics on burrowing behavior

by Kelly M. Dorgan[1,2], Sanjay R. Arwade[3] and Peter A. Jumars[1]

ABSTRACT

Recent studies document linear elastic response of muddy marine sediments to load and deformation on temporal and spatial scales relevant to animal movement, with burrowers making openings for movement in such sediments by fracture. Cracks propagate through linear elastic solids in mode I (opening-mode crack growth) when the stress intensity factor (K_I) at the crack tip exceeds the material's fracture toughness (K_{Ic}). Fracture mechanics depend on material stiffness as well as fracture toughness, and we prepared a range of transparent gels that varied in stiffness and fracture toughness to assess the dependence of burrowing behavior on these material properties. When the polychaete *Nereis virens* elongated its burrow, it altered its body shape and behavior across these gels in a manner consistent with fracture mechanics theory. We modeled burrow elongation as stable, wedge-driven crack growth, and calculated that K_I values at the tips of the burrows reached K_{Ic} values of most gels without pharynx eversion and exceeded K_{Ic} when the pharynx was everted. In materials with higher fracture toughnesses, worms everted their pharynges to become thicker and blunter wedges, as predicted from simple wedge theory. In stiff materials with low toughness, worms moved their heads from side-to-side to extend crack edges laterally, relieving elastic forces compressing them and allowing them to maintain body shape more easily. This solution extends the crack in small increments that each require relatively little force. We introduce a dimensionless "wedge" number to characterize the relative importance of work to fracture the material and extend the burrow and work to maintain body shape against the elastic restoring force of the material. The mechanism of burrowing by crack propagation is utilized across a range of material properties found in natural muds, and variation in these properties strongly influences burrowing behaviors. These results demonstrate how quantifying the mechanical properties of muds can improve our understanding of bioturbation. On spatial and temporal scales relevant to burrower activity, variations in these properties may impact particle mixing by influencing burrower behavior.

1. Introduction

Burrowing animals are ecosystem engineers, altering habitat structure by moving through, ingesting and egesting sediments (cf. Meysman *et al.,* 2006). Extensive literature documents dependence of benthic community structure on sediment properties, primarily grain size and organic content (e.g., Gray, 1974; Ramey and Snelgrove, 2003). Recently,

1. Darling Marine Center, University of Maine, 193 Clark's Cove Road, Walpole, Maine, 04573, U.S.A.
2. Present address: Department of Integrative Biology, University of California-Berkeley, Berkeley, California, 94720, U.S.A. ***email: kelly.dorgan@berkeley.edu***
3. Department of Civil and Environmental Engineering, University of Massachusetts, Amherst, Massachusetts, 01003, U.S.A.

we have identified the sediment mechanical variables that determine the capability of animals to burrow in muds by means of crack propagation (Dorgan *et al.,* 2005, 2006). Here we begin an examination of the potential feedbacks between sediment mechanics and behavior by asking whether worms alter their burrowing behaviors as those sediment mechanical variables assume different values.

Sediments exhibit a dramatic variety of material properties, ranging from granular materials such as clean, monodisperse sands to linear elastic materials such as some, and perhaps most, muddy sediments. Differences in material properties result in differences in burrowing behavior in different sediments (Dorgan *et al.,* 2006), and burrowing may have evolved first in sands with granular mechanics (Jumars *et al.,* 2007). The polychaete *Nereis virens* burrows through muddy marine sediments by crack propagation (Dorgan *et al.,* 2005), and this mechanism is likely widespread in muds (Dorgan *et al.,* 2006). The burrow is a planar crack (shaped much like a tongue depressor) that extends laterally as well as anteriorly away from the worm, which is compressed dorsoventrally by the elastic walls of the burrow (Dorgan *et al.,* 2005). The worm exerts a dorsoventral force against the burrow walls, and the resulting stress in the sediment is amplified at the crack tip.

Linear elastic fracture mechanics theory considers three material properties for two-dimensional problems in which the material is isotropic and the crack is loaded only in mode I, the crack opening mode (i.e., with the material in uniaxial extension): elastic modulus or stiffness (E), critical stress intensity factor or fracture toughness (K_{Ic}), and Poisson's ratio (ν). The stiffness (force L^{-2}) relates stress, σ (force L^{-2}), and strain, ε (elongation (L)/original length (L)), as $\sigma = E\varepsilon$ in a linear elastic, isotropic material undergoing uniaxial deformation. Poisson's ratio (dimensionless) is defined as the negative of the constant of proportionality between longitudinal and transverse strain under uniaxial stress. For incompressible materials, Poisson's ratio is equal to 0.5; lower values of ν indicate higher compressibility. Mode I stress intensity, K_I (force $L^{-1.5}$), is the coefficient of the dominant term in the series expansion of the stress field at a crack tip under mode I loading and is used to compare stresses at cracks of varying configurations under varying loading conditions. The crack propagates when K_I exceeds the critical value, K_{Ic}, the fracture toughness of the material. Another way of stating the fracture criterion is that when energy release rate, G (energy L^{-2}), exceeds resistance of the material, R (energy L^{-2}), the crack grows. If energy release rate increases as the crack grows, growth is unstable (e.g., shattered glass), whereas if energy release rate decreases as the crack grows, growth is stable and stops when energy release rate falls below material resistance. Displacement- or wedge-driven fracture is often stable, whereas load-driven fracture is often unstable. Relevant fracture mechanics have been recently reviewed in biomechanical contexts (cf. Dorgan *et al.,* 2006, 2007; Mach *et al.,* 2007) and can be found in engineering texts (e.g., Anderson, 1995).

According to linear elastic fracture mechanics (LEFM) theory, the ratio of fracture toughness (K_{Ic}) to stiffness (E) determines the shape of bubbles that grow by fracture in elastic media (Johnson *et al.,* 2002; Boudreau *et al.,* 2005). Growth of bubbles in muddy sediments has been modeled using LEFM (Johnson *et al.,* 2002; Boudreau *et al.,* 2005),

and LEFM has been applied to burrowers as well (Dorgan *et al.,* 2007). This ratio, K_{Ic}/E, is also important to burrowers and has been assumed to affect burrow shape and consequently burrowing behavior. Forces exerted by *Nereis virens* during pharynx eversion were measured in seawater gelatin, used as an analog for muddy sediments because their ratios of K_{Ic}/E are similar (Johnson *et al.,* 2002; Dorgan *et al.,* 2007). The pharynx, or "throat" region, is everted both for feeding and burrowing; during burrowing, the pharynx acts much like a balloon expanding the anterior region of the worm and exerting forces against the dorsal and ventral crack walls (cf. Dorgan *et al.,* 2005). Finite element modeling was used to convert forces measured in gelatin to those exerted by *N. virens* in natural sediments. Calculated forces are much lower than those previously measured (cf. Hunter and Elder, 1989) and are directly proportional to the stiffness (E) of the material. Although few data on sediment stiffness exist (e.g., Johnson *et al.,* 2002; Dorgan *et al.,* 2007), existing data agree with qualitative observations (e.g., how far one's boots sink when walking at low tide) of extensive variability in mud stiffness. Not only does E vary among sediments and with depth in sediments, but K_{Ic} likely varies extensively as well, and these variations and their dependence on properties such as grain size, porosity and organic polymer content are poorly understood.

To address the question of whether variations in mechanical properties of muddy sediments, specifically in the ratio K_{Ic}/E, affect burrowing kinematics, we developed transparent polymer gels with various fracture toughnesses and stiffnesses and quantified burrowing behavior of *Nereis virens* in them. From fracture mechanics theory, the shape of a wedge that extends a crack stably also depends on the ratio of K_{Ic} to E; the higher K_{Ic}/E, the thicker and blunter the wedge (Sih, 1973). We predicted that the shapes of burrowing worms would depend on this ratio and modeled worms as wedges to calculate K_I.

We used stiffness and fracture toughness, material properties of elastic solids such as marine muds, to develop a dimensionless "wedge" number. The wedge number compares the work of fracture to extend the burrow and the work to move forward and deform an elastic medium. The Reynolds number, which incorporates fluid parameters of density and viscosity in a ratio of work against inertia to work against viscosity, has provided great insight to differences in swimming behaviors among animals moving at different Re. An analogous tool for burrowing behavior, as developed here, has only recently become possible with advances in the understanding of sediment mechanics (e.g., Johnson *et al.,* 2002).

2. Materials and methods

a. Animals

Specimens of *Nereis virens* ($\sim$ 6–8 cm length) were collected from an intertidal mudflat in Edgecomb, ME, at low tide and kept under flowing seawater until used in experiments. Range of worm sizes was restricted deliberately to avoid confounding of size-specific behaviors with changes due to material properties.

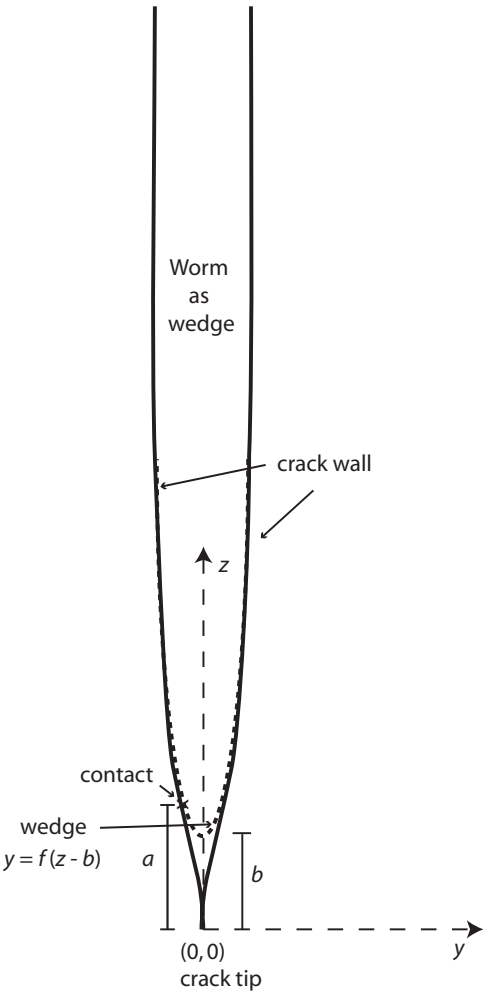

Figure 1. Wedge of arbitrary profile (dotted line) extending a crack (solid line) by stable crack growth. The schematic represents a worm burrowing downward. The wedge profile is given by $y = \pm f(z - b)$, where b is the distance between the crack tip and the anterior end of the worm, and a is the distance between the crack tip and the contact of the wedge with the crack wall (adapted from Sih, 1973).

b. Relevant fracture mechanics theory and predicted implications for burrowing behavior

We observed in our kinematic analysis of *N. virens* burrowing in gelatin that the crack extends anteriorly only when the worm is moving forward, i.e., the worm's body is a wedge driving the crack growth (Dorgan *et al.,* 2007). The analytic solution for the stress intensity factor at the tip of a stable crack produced by a 2D wedge of arbitrary profile (Fig. 1) is

$$K_I = \frac{E\sqrt{2a}}{2\sqrt{\pi}\,(1-\nu^2)} \int_a^\infty \frac{f'(z-b)}{\sqrt{z(z-a)}}\,dz, \quad a > b \text{ (Sih, 1973).} \tag{1}$$

As shown in Figure 1, $y = \pm f(z - b)$ is the wedge profile, or worm thickness, and b is the distance between the crack tip and the tip of the wedge. The distance between the crack tip and the contact with the wedge, a, is calculated based on the assumption that crack growth is stable. Eq. (1) can be used to calculate the stress intensity generated by a worm of known shape. (N.B.: To obtain Eq. (1), the equation for k_1 given by Sih (1973; Section 1.2.9, p. 4) was multiplied by $\sqrt{\pi}$ to conform with modern notation for K_I. In addition, the equation was rewritten in terms of E and ν. The coordinate system was changed from x-y to y-z to correspond with the 3D coordinate system used for experiments (the same as in Dorgan *et al.,* 2007) in which the z-axis is vertical).

Considering a worm as a wedge, b is the distance between the anterior end of the worm and the anterior end of the burrow, and $(a - b)$ is the distance between the anterior end of the worm and the dorsoventral contact of the body with the crack wall. To fit the relatively simple model of Eq. (1), the wedge must be symmetrical about the z-axis, whereas the dorsal and ventral sides of a worm are not identical; when the worm is moving straight, however, the shape is approximately symmetrical (cf. Dorgan *et al.,* 2005, Fig. 1c). In addition, the wedge is assumed to be infinitely long, whereas worms clearly are not. As z increases (toward the posterior of the worm), the term, $\sqrt{(z(z-a))}$ increases, and the slope of the worm's body surface (relative to a line parallel to z) approaches zero. The posterior region of the worm therefore contributes little to K_I.

It is possible to obtain b from video, either by direct visualization of the crack tip or by assuming that when the worm is moving forward $b = 0$, and when the anterior end of the worm moves backward, b is the distance between the anterior end and the previously farthest anterior point of advance. However, neither a nor $(a - b)$ can easily be obtained from video analysis of worms burrowing.

To solve the problem of one equation (Eq. 1) in two unknown variables (a and K_I), another equation was needed. Equation (1) was derived from the combination of two equations (containing three unknowns; Barenblatt, 1962),

$$h - \int_a^\infty f'(z-b)\,\sqrt{\frac{z-a}{z}}\,dz = \frac{K_I\sqrt{2\pi a}\,(1-\nu^2)}{E} \text{ (his Eq. 6.10) and} \tag{2}$$

$$h = \int_a^\infty f'(z-b)\,\sqrt{\frac{z}{z-a}}\,dz \text{ (his Eq. 6.8).} \tag{3}$$

Here, h, the third unknown, is the half thickness of the wedge at infinity. Since we can measure h (the half thickness of the worm's body) from video, we now have two equations (Eqs. (1) and (2)) and two unknowns (a and K_I). (N.B.: To obtain Eq. (2), 'K' in Eq. 6.10 (Barenblatt, 1962) was multiplied by $\sqrt{(\pi/2)}$ to conform with the modern notation for K_I.

In Eqs. (2) and (3), the y-z coordinate system that we use throughout replaces the x-y coordinate system used by Barenblatt (1962).) Solving Eq. (2) for K_I gives

$$K_I = \frac{E}{\sqrt{2\pi a}\,(1-\nu^2)}\left(h - \int_a^\infty f'(z-b)\,\sqrt{\frac{z-a}{z}}\,dz\right). \tag{4}$$

K_I and a were obtained by solving Eqs. (1) and (4), a system of integral equations in a and K_I, iteratively. A simple iterative scheme suffices in which an initially small value of a is increased until Eqs. (1) and (4) yield values of K_I that agree within a tolerance of 2 Pa $m^{0.5}$. The average of the two K_I values is then taken as the solution. This simple approach is possible because elasticity theory guarantees a unique solution to Eqs. (1) and (4) (Timoshenko and Goodier, 1970).

We have shown that a 2D, plane strain, finite element model of the lateral view of *Nereis virens* burrowing in gelatin is a reasonable approximation for the 3D geometry of the worm when it is extending a crack-shaped burrow (Dorgan *et al.,* 2007). This same approximation is made in applying the 2D wedge equation. The assumptions in applying a 2D plane strain model are that the dorsoventral thickness of the worm is constant over the entire lateral width of the worm and that the width is large enough that the stress field around the body is unaffected by the lateral edges of the crack and is instead constant through the width of the worm. In other words, a 2D, sagittal section through the middle of the worm (showing an anterior to posterior profile of thickness and applied stresses) adequately represents the displacements and stress field across the entire width of the worm. In gelatin, *N. virens* moves its head from side-to-side, extending the crack laterally, and we have suggested that this behavior is important in enabling approximation of the burrow as a 2D plane strain geometry because it moves the effect of the lateral edge of the crack away from the worm, making the stress field around the worm more constant across the width of the worm (Dorgan *et al.,* 2007).

Application of the wedge equation was tested by using measured shapes of large nereidids burrowing in gelatin, for which K_I was calculated through finite element modeling from measured forces (data from Dorgan *et al.,* 2007). From the finite element model, K_I varied from 57 to 64 Pa $m^{0.5}$ (Dorgan *et al.,* 2007), and from the wedge equation (Eqs. (1) and (4)), K_I was 54 Pa $m^{0.5}$. K_{Ic} for gelatin is 50-220 Pa $m^{0.5}$ (Johnson *et al.,* 2002). These two methods differ substantially: the finite element modeling method calculates K_I from the stresses applied, whereas the analytical wedge equation calculates K_I from the applied displacements using the material stiffness. The similar results from the two methods indicate that the analytical wedge equation is as applicable as previously used finite element analysis. Use of photoelastic stress analysis to measure forces exerted by burrowing worms, as required for application of the finite element method (cf. Dorgan *et al.,* 2007), is limited to large worms that exert large forces while burrowing in clear materials. The wedge equation enables calculation of K_I for small worms burrowing in more opaque materials and thus expands greatly the range of media for which mechanical analysis is feasible.

Another advantage of using an analytical solution rather than finite element modeling to calculate K_I is the ability to make predictions from the equations. From Eq. (1), the stress intensity factor increases in direct proportion to the stiffness of the material, following intuition, because the stiffer the material, the larger the stresses that must be exerted on the crack faces by the wedge to maintain displacements compatible with the wedge profile. In other words, the ratio K_I/E is determined by the shape of the wedge. This dependence is consistent with the dependence of bubble aspect ratios on K_{Ic}/E; as K_{Ic}/E increases, the aspect ratio of a bubble increases (cf. Johnson *et al.,* 2002). Similarly, a wedge will have to change shape to have a higher K_I/E that reaches the critical value, consistent with our expectation that shape and even behavior within the burrow also depend on this ratio. Bubbles that grow by fracture essentially act as oblate spheroidal wedges, so the dependence of bubble and wedge shapes on the same ratio is unsurprising. Wedges with steeper slopes, i.e., blunter fronts, particularly near the point of contact with the crack wall (at $z = a$, cf. Fig. 1), will generate higher stress intensity factors. From Eq. (4) comes the intuitive prediction that a thicker wedge (larger h) will have a higher stress intensity factor, just as a bubble with a larger aspect ratio exerts a higher K_I (cf. Johnson *et al.,* 2002). It creates higher tensile stress perpendicular to the crack direction.

Considering worms as wedges, we can make both qualitative and quantitative predictions about how burrowing behavior depends on the mechanical properties of sediments. As K_{Ic}/E increases, the stress intensity factor (normalized to E) from the wedge shape must increase in order for the crack to propagate. The most obvious way to increase the stress intensity factor is through pharyngeal eversion. The worm uses internal pressure to evert the pharynx, or throat region, extending it anteriorly and exposing jaws and adhesive mucus used in feeding. Pharyngeal eversion increases thickness of the wedge near the crack tip as well as the slope of the anterior end near the contact with the crack wall. Although worms are physiologically constrained to a range of body shapes, their hydrostatic skeleton enables some variation in body thickness and in the shape of the anterior region. For example, driving the body forward into the crack would increase the thickness and the slope of the head region. Both body thickness and slope (of the head) at the point of contact (the distance a from the crack tip) are expected to be larger in materials with greater fracture toughness-to-stiffness ratios. The null hypothesis was of no change in body shape (or change opposing this prediction) with solid mechanical properties of the sediment, tested against the one-tailed alternative of thicker and blunter shape as K_{Ic}/E increased. We also predicted that stress intensity factors calculated from lateral views of burrowing worms would differ in gels with different fracture toughnesses and would be close to the critical stress intensity factors for the gels in which they were burrowing.

c. Gels

Five polymer gel recipes were developed that appeared homogeneous (i.e., no precipitate or obvious heterogeneity), were transparent enough to see worms clearly in a 500-mL aquarium, and in which worms were able and willing to burrow (Table 1). The five recipes were selected to be approximately isosmotic with seawater and non-toxic. Gels were all

Table 1. Gel recipes.

Material	Gelatin	Gelatin/ ι-carrageenan	Gelatin/ agar	κ-carrageenan/ glucomannan	Gelatin/ LA gellan gum
Ingredients	28.35 g L^{-1} gelatin	28.35 g L^{-1} gelatin 5.0 g L^{-1} ι-carrageenan	28.35 g L^{-1} gelatin 5.0 g L^{-1} agar	4.8 g L^{-1} κ-carrageenan 1.2 g L^{-1} glucomannan	14.18 g L^{-1} gelatin 1.5 g L^{-1} LA gellan gum
Hydration		Stir for 20 min	Stir for 12 min	Stir for 20 min	Hydrate in tap water

kept in a cold room at 11°C during experiments. First, we used gelatin (www.bulkfoods.com), 28.35 g (L seawater)$^{-1}$. Gelatin appeared stiffer than in previous experiments (Dorgan *et al.,* 2005, 2007) due to wall effects in smaller aquaria, although the concentrations were the same. Gelatin was mixed in 500 mL seawater and brought to a boil, mixing continually.

For the second gel, gelatin (28.35 g (L seawater)$^{-1}$) was mixed with 5 g (L seawater)$^{-1}$ ι-carrageenan (FMC Biopolymer, Philadelphia, PA), added to seawater and stirred for 20 min to fully hydrate the carrageenan, then brought to a boil. Gelatin is synergistic with ι-carrageenan but not κ-carrageenan (Philips and Williams, 2000), and the mixture of gelatin and ι-carrageenan is qualitatively similar but more transparent than the more commonly used mixture of κ- and ι-carrageenan; ι-carrageenan gels are less stiff and tougher than κ-carrageenan gels, and mixing the two varieties in varying proportions yields gels with intermediate properties (Philips and Williams, 2000). This gel started to set almost immediately and was poured into aquaria within a minute after being removed from heat. Waiting longer resulted in a heterogeneous gel. To prevent cracking the glass, aquaria were placed in a container of hot water and allowed to equilibrate before the hot liquid was added.

For the third gel, gelatin (28.35 g (L seawater)$^{-1}$) was mixed with 5 g (L seawater)$^{-1}$ agar (www.bulkfoods.com), added to seawater and stirred for 12 min to fully hydrate the agar, then brought to a boil.

For the fourth gel, 4.8 g (L seawater)$^{-1}$ κ-carrageenan (FMC Biopolymer, Philadelphia, PA) was mixed with 1.2 g (L seawater)$^{-1}$ glucomannan (or konjac mannan, Starwest Botanicals, Cordova, CA), added to seawater, stirred for 20 min to fully hydrate the carrageenan, then brought to a boil. Addition of glucomannan to κ-carrageenan, a stiff, brittle gel, results in a much tougher gel (Philips and Williams, 2000). We initially tried higher concentrations of this mixture as well as higher proportions of glucomannan, but worms were either unable to burrow or moved too slowly and stopped too frequently to obtain useful data. We therefore consider this gel to be near a limit of fracture toughness for *Nereis virens* of the size range used in experiments.

For the fifth gel, gelatin (14.18 g L^{-1}) was mixed with 1.5 g L^{-1} low acyl (LA) gellan gum (Kelcogel F, CP Kelco U.S., Chicago, IL) and added to tap water and stirred and brought to a boil. Once the solution boiled, salts were added to make 35 salinity artificial seawater. The LA gellan gum does not hydrate in the presence of salts, instead forming a precipitate and settling, but salts are needed for cross-linking and are added after hydration.

LA gellan gum is a stiff, brittle gel that is synergistic with gelatin (Philips and Williams, 2000).

Aquaria were built with glass sides (enabling use of polarizing filters) and plexiglass bases with inside dimensions 0.072 m wide × 0.072 m deep × 0.10 m high. This size was chosen so the worms could be seen clearly in the most opaque gel, the κ-carrageenan and glucomannan mixture. Small holes were drilled in the centers of the plexiglass bases for fracture toughness measurements and were covered with silicone sealant before gels were added.

d. Mechanical testing of gels

i. Elastic modulus. A Vitrodyne V-1000 microtensile tester was used to measure force and displacement as a probe was lowered onto the surface of the gels in the aquaria (some replicates were in round beakers of the same surface area and height as the aquaria). Finite element analysis provides the calibration factor for computing E from the measured force-displacement response. Several replicate measurements (N = 4-8) were taken using two different probes (0.0126 m and 0.0047 m radii), and results were averaged. Stiffness measurements were not conducted in the cold room, but gels were kept as close to 11°C as possible.

Although an analytical solution exists for the elastic modulus as a function of displacement and force exerted by a rigid cylinder resting on the surface (cf. Dorgan *et al.,* 2007), that solution assumes that the material is a semi-infinite solid (i.e., no wall effects). Because the aquaria are small (0.072 m × 0.072 m × 0.1 m deep), the walls do affect measured or apparent material stiffness. To account for the wall effect, we instead modeled the probe on the surface of an aquarium (with rigid walls) using the finite element modeling program, franc2d (Cornell Fracture Group). Displacements of 0.002 m were applied along the radius of each of the two probes in a 2D axisymmetric model, and the model was used to obtain stress as a function of r. Although the aquaria are rectangular, the axisymmetric model required the geometry to be approximated as a cylinder. We chose a radius, r = 0.0395 m, to give equal surface areas between the modeled and actual aquaria (close to radius 0.04 m of beakers). A line plot of stress along the probe contact was obtained from franc2d, and the stress was integrated over the area of the probe to calculate the force exerted. Because we obtained surface stresses on the bottom face of the probe, σ_i, at n discrete points, r_i, in the finite element model, we used a summation

$$F = \sum_{i=1}^{n} \sigma_i(\pi(r_{i+1}^2 - r_i^2)), \tag{5}$$

rather than integration to find the total force applied to the probe.

The force required to displace the probe 0.002 m is a linear function of stiffness. This procedure was repeated for three values of stiffness to ensure linearity, and a linear regression between calculated force and the three values of stiffness was obtained. (Because calculated force depends directly on stiffness, the three points fell on the same

line.) This regression was then used to convert forces measured with the Vitrodyne tester at 0.002 m displacement to apparent stiffnesses of the gels in aquaria with rigid walls.

ii. Fracture toughness: Method 1. Fracture toughness was measured by injecting a bubble into the gel, measuring bubble pressure, and using the solution for the stress intensity factor for a penny-shaped crack with internal pressure. This solution, from the principle of superposition, is equal to the solution for a penny-shaped crack with far-field stress,

$$K_I = \frac{2}{\sqrt{\pi}} \sigma \sqrt{a_{bub}} \tag{6}$$

where a_{bub} is the principal radius (half-length) of the bubble, and σ is the far-field stress (Sih, 1973).

Water was injected through a (25G) needle inserted through the hole in the bottom of the aquarium to form a liquid "bubble" (Fig. 2). The needle was attached to, on one side of a valve, a syringe to initiate the bubble, and on the other side, a pressure transducer (that measured the internal pressure of the bubble) and a syringe dispenser. The setup was attached to a micromanipulator used to insert the needle into the gel. Because we expected the pressure needed to initiate a bubble to be greater than the upper limit of the transducer, the bubble was started with the valve to the transducer closed. Then, once the bubble formed, the valve was switched and the bubble was grown in increments with the dispenser. Two CCD cameras recorded the shape of the bubble from 90° angles and were lined up to capture views perpendicular, respectively, to the major and minor axis of the oblately spherical bubble. Photographic light tables were placed on opposite sides of the aquarium from the cameras, and the cameras and lights had crossed polarizing filters to more easily visualize the bubble (cf. Dorgan *et al.,* 2007). For more opaque materials, the polarizers were lined up to allow more light to pass through the gel. The bubble made a penny-shaped crack with the plane oriented roughly 10–15° from vertical.

The pressure peaked when water was added, and as the bubble started to grow its pressure decreased toward an asymptote (Fig. 3A). This constant pressure, P_{tot}, reached after the bubble stopped growing, was used to obtain σ_c. Because the bubble was vertical, a pressure gradient existed between the crack tip at the top of the bubble and the needle; the pressure difference, P_{hydro}, calculated from the height difference (cf. Fig. 2), was subtracted from the pressure transducer reading. A baseline pressure, P_{base}, recorded both before the needle was inserted and after the needle was removed (labeled 'b' in Fig. 3A), was also subtracted from the pressure transducer reading. Occasionally, the pressure did not drop as low as the initial baseline pressure after the needle was removed, possibly due to a clog in the needle, in which case only the initial baseline was used. The critical pressure,

$$\sigma_c = P_{tot} - P_{hydro} - P_{base} \tag{7}$$

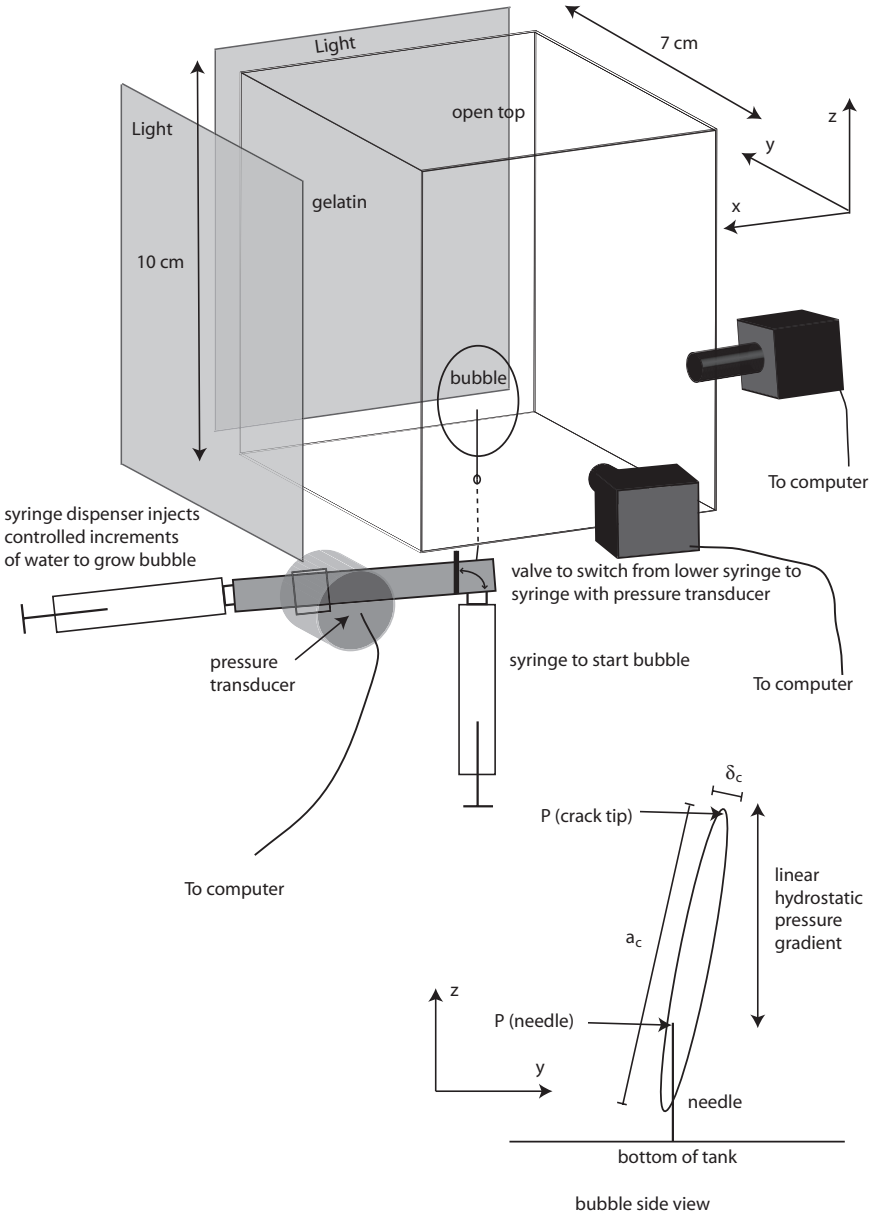

Figure 2. Schematic of liquid or bubble injection. A needle is inserted through a hole (covered with silicone sealant) in the bottom of an aquarium of gel with the valve closed to the pressure transducer. A bubble is initiated with the lower syringe to protect the pressure transducer from the relatively high pressures needed to initiate the bubble. Once the bubble forms, the valve is switched, and the bubble is grown incrementally with the syringe dispenser. Two cameras set up at 90° capture images each time the bubble is grown (once growth stops and pressure stabilizes). A hydrostatic pressure gradient exists between the crack tip and the needle (where the baseline pressure is measured), and that difference is removed during analysis.

was used to calculate K_{Ic} from Eq. (6). K_{Ic} was calculated as the slope of the linear regression between $\sqrt{a_{bub}}$ (x-axis) and $(\sqrt{\pi})/(2\sigma_c)$ (y-axis). This regression was forced through the zero intercept.

In the κ-carrageenan/glucomannan gel, the water-filled bubble could not be seen even with the polarizing filters. Because the length of the bubble was necessary to calculate K_{Ic}, we used air instead of water to create an easily visualized bubble. For air bubbles, the vertical pressure gradient is very small ($P_{hydro} \approx 0$), and only the baseline pressure was subtracted. Bubbles did not grow in initial experiments in which air was added with the dispensing syringe (cf. Fig. 2), likely because the material was too tough. We instead used

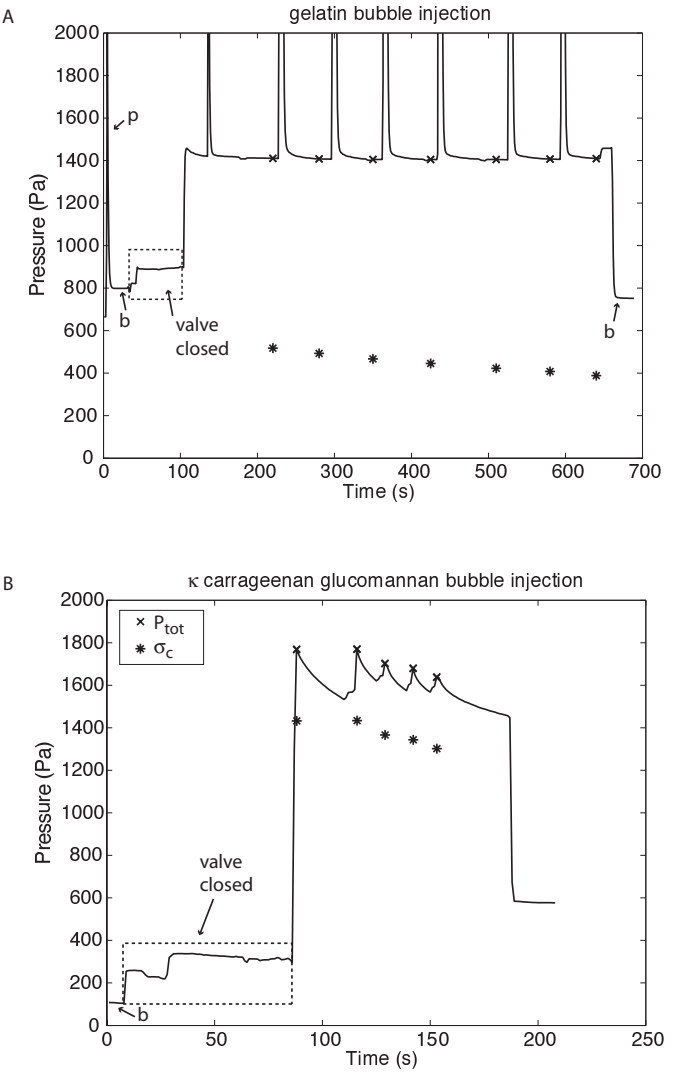

only the lower syringe (used only to initiate bubbles in other materials) to add air to grow the bubble, turning the valve to measure the pressure with the pressure transducer as quickly as possible after adding air. Because pressure was not measured as air was added to the bubble, the pressure peak observed in the other gels was not captured. Instead, the pressure peaked when the valve opened, then slowly decreased at a fairly constant rate, during which time the bubble did not grow. (In other materials, the bubble slowly extended as the pressure dropped (Fig. 3B).) We believe that the drop in pressure was due to creep because as the pressure dropped, an imprint of the previous bubble (thicker than the extended part) slowly disappeared. We considered the initial maximum pressure when the valve was opened to the pressure transducer to be P_{tot}, but this value slightly underestimates σ_c because of the drop in pressure that occurred between the time the bubble stopped growing and the valve was opened. Calculated K_{Ic} for this gel is therefore likely slightly underestimated using method 1.

iii. Fracture toughness: Method 2. Fracture toughness was also calculated from aspect ratios of the bubbles. The two cameras were oriented to view the bubble injected in method 1 straight on (the head or tail of the 'penny') and at 90° (to measure thickness). The aspect ratio was calculated from the bubble thickness and length. The aspect ratio of the bubble, a penny-shaped crack, is

$$\frac{\delta_c}{a_c} = \frac{2(1-\nu^2)K_{Ic}}{\sqrt{\pi}\, E a_c^{1/2}} \tag{8}$$

δ_c is the displacement or half-thickness of the bubble and a_c is the half-length of the bubble (labeled on Fig. 2). (Eq. (8) is similar to Johnson *et al.,* 2002 Eq. 19, corrected based on Fett, 1982; confirmed by personal communication with B. P. Boudreau). K_{Ic} was

←

Figure 3. Pressure record during bubble injection in (A) gelatin and (B) κ-carrageenan/ glucomannan. A: In gelatin, a flat baseline (b) follows an initial peak (p) created by adjustment of the needle; then the valve is closed, causing the pressure to increase. The bubble is injected while the valve is closed, and when the valve is opened, the pressure increases rapidly. A small amount of water is added immediately (the peak before the first x) to ensure that the pressure in the bubble is at σ_c, and when the pressure levels out, images are captured and the pressure is recorded, from which the hydrostatic pressure and baseline are subtracted to obtain σ_c. A peak occurs each time the bubble is grown, and a pressure recording is taken each time the pressure levels out (indicated with x's). The needle is then removed and a second baseline (b) is recorded (to be averaged with the initial baseline). Corrected pressures (σ_c) are indicated with *'s. B: In κ-carrageenan glucomannan, air rather than water was used for injection. The initial baseline (b) is lower than for the water bubble because the water does not extend up the needle. The valve is closed after the baseline is obtained; then the bubble is initiated. When the valve opens, the pressure peaks, then decreases due to creep. The valve is closed, and the bubble grown. When the valve opens again, another pressure peak is observed. In this bubble injection, the baseline did not drop as low as the original baseline, so only the first baseline was used.

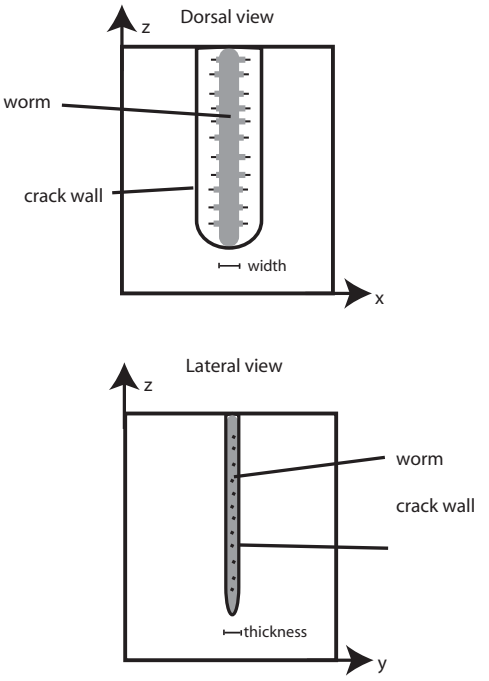

Figure 4. Schematic of the coordinate system used in analysis. The lateral view image shows the worm as a wedge (as in Fig. 1).

calculated for each aquarium as the average of K_{Ic} values for bubbles in which both length and thickness could be clearly seen in images.

Because of the creep in the κ-carrageenan/glucomannan, the thickness of the bubble may have been overestimated, leading to overestimation of K_{Ic} (contrasted with underestimation by method 1 in this gel).

e. Experimental design for burrowing experiments

After bubble injection, a worm was added to the aquarium and placed in a crack made with forceps, as in previous experiments (Dorgan *et al.,* 2005, 2007). Worms were initially placed with their heads pointed downward in the crack to encourage burrowing, and were returned to that orientation if they backed out or turned around and moved up toward the surface of the crack. Video was recorded with cameras on two sides of the aquarium (cf. Fig. 2, modified from Fig. 1 of Dorgan *et al.,* 2007) once worms began burrowing. Segments of video were selected for both dorsal (or ventral) and lateral view analyses (Fig. 4). For a video segment to be used, the worm had to be burrowing within the plane of view of the camera rather than moving toward or away from the camera ($< 30°$ from vertical with respect to the view from the other camera). Other criteria for selection were that the camera was not moving and the worm was in focus.

After a worm burrowed, it was preserved in formalin, and later the width of the 4th

setiger was measured from the ventral side of the worm. This width was used to calculate normalized pharynx and body thicknesses to compare among worms burrowing in different gels. Preserved body lengths and wet weights were also measured. ANOVA for differences in mean length, width, and weight of worms in each gel ensured that worms of similar size were used in the different materials.

f. Video analysis: dorsal/ventral view

Dorsal view video segments were used to measure velocity, time and distance traveled in each cycle of lateral head movement and pharyngeal eversion, and the lateral distance moved by the anterior end of the worm. The lateral distance is an indication of how far the burrow extends laterally away from the worm and hence an indication of relief of stress from elastic rebound of the material.

For segments of video showing a direct dorsal view, x-z coordinates of the center of the anterior end of the worm were obtained for a sequence of frames. A second-order polynomial was fitted through the x-z coordinates to separate forward progress from lateral head movements. Distance traveled for each frame was calculated as the length of the polynomial curve from the initial frame. Lateral movements of the anterior end of the worm over time were calculated as residuals from the best-fit polynomial.

Video segments were then classified into one of the following behavioral categories: (1) periodic, side-to-side head movements without pharynx eversions, (2) pharynx eversions with irregular or no head movements, or (3) pharynx eversions with periodic, side-to-side head movements. Further analysis differed for the three categories of behavior. Most worms exhibited only one of the three; one worm burrowing in gelatin/agar exhibited more than one behavior in sequences long enough for analysis and was included in both behavior categories.

For video segments in which the worm exhibited periodic, side-to-side head movements without pharyngeal eversions, we calculated the period of head movement, lateral distance of head movement, forward distance traveled per cycle of head movement, and velocity. The period of head movement (s cycle^{-1}) was determined by first removing the best-fit second order polynomial then finding the peak in the Fourier-transformed, polynomial-detrended data. The inverse of the peak frequency is the period of head movement. Video segments of less than three complete cycles were excluded. Average lateral distance of head movement was calculated as the average of the peaks of the residuals, doubled to obtain the full amplitude. Only peaks between two zero intercepts were included. (For example, if the worm's head was initially on the left side, an initial left peak was excluded, and measurement started with the first right peak.) Lateral distance of head movement was normalized for comparison of worms among gels by dividing by the width of the worm (m/m). Velocity was calculated as the slope of the best-fit line of distance traveled as a function of time. Distance traveled per cycle was calculated as the product of the period of the cycle and the velocity. When more than one video segment was analyzed for a worm, weighted averages of periods and lateral distances of head movements, forward distances

per cycle and velocities were calculated for that worm based on the number of cycles of head movement in each video segment.

For video segments in which the worm exhibited pharyngeal eversions with irregular or no head movements, the period of pharynx eversions, distance traveled between eversions, and resulting velocity were calculated. Pharynx eversions resulted in peaks in a plot of distance traveled as a function of time (because the pharynx rapidly extended anteriorly, then was retracted, decreasing the distance traveled). The period of pharynx eversions was calculated as the time between those peaks, and the distance traveled per cycle was calculated as the distance between peaks. Velocity was then calculated as the distance per cycle divided by the period of the cycle. Because period, distance, and velocity were all calculated from individual cycles, the average for each worm was simply the average of the observations.

For video segments in which the worm exhibited pharyngeal eversions with periodic side-to-side head movements, the period of pharynx eversions, distance traveled per cycle, and velocity were calculated as for the worms exhibiting pharyngeal eversions without periodic head movements. In addition, we calculated the period and lateral distance of head movements. Because the head movements alternated with pharynx eversions, calculating periods from Fourier-transformed residuals did not work. Instead, the period and distance traveled were measured directly for individual cycles of head movement from plots of forward distance traveled as a function of time. The calculated distances and periods of head movements exclude the pharynx eversion part of the cycle, whereas distances and periods of pharynx eversions include the head movement part of the cycle.

g. Video analysis: lateral view

Lateral-view video segments were used to calculate K_I from the wedge equation. For video segments in which the worm everted its pharynx, sequences of frames around the pharynx eversion were analyzed, whereas for video segments without pharynx eversion, individual frames were analyzed. Stress intensity factors (K_I) and points of contact with the crack wall (a) were calculated from measured worm thicknesses by solving Eqs. (1) and (4) in Matlab 7.4.0 (R2007a; The Mathworks, Inc., Natick, MA, USA). The slope of the anterior region at the point of contact was also calculated. For sequences of images around a pharynx eversion, the peak K_I was identified.

For segments of video showing a direct lateral view, individual frames were captured, and for each frame thicknesses were measured at 10 different distances from the anterior of the worm with LabView. The 10 distances at which thicknesses were measured were not identical because the lengths of worms visible in frames differed, and distances were chosen to cover the entire visible length. The shape of the worm was determined by interpolating from those 10 thicknesses using a cubic spline function in Matlab. The thickness of the worm (the average of the posterior two data points) was extended out to 0.02 m length for consistency in comparing data from frames with thicknesses measured at different distances.

Normalized pharynx thickness, normalized body thickness, distance to contact with the

crack wall (a), and the slope at contact were averaged for each material for comparison among gels. Pharynx thicknesses were measured as the maximum thickness along the anterior 0.002 m of the worm. For this comparison, pharynx and body thicknesses were normalized to worm size by multiplying by the average width of all worms and dividing by the width of the individual worms. (Real thicknesses were used to calculate K_I and a.)

3. Results

a. Animals

Worms used in experiments had preserved length of 3.4 ± 0.5 cm (mean ± S.D., N = 37), width of the 4th setiger of 1.7 ± 0.2 mm, and wet weight of 107 ± 41 g. Worm size did not differ significantly among the five gels. (F-values for an ANOVA test for differences in means were $F_{4,34} = 0.44$, $F_{4,34} = 0.45$, and $F_{4,34} = 0.96$ for length, width, and wet weight, respectively, with corresponding p values of 0.78, 0.77 and 0.44.)

b. Gel mechanics

Stiffnesses were similar for gelatin (7,100 ± 372 Pa; mean ± S.D., N = 8), gelatin/ι-carrageenan (6,880 ± 1,464 Pa, N = 5), and κ-carrageenan/glucomannan (8,258 ± 1,218 Pa, N = 6) (Table 2). Gelatin/agar was significantly stiffer (16,855 ± 1,671 Pa, N = 6) than other materials (although the difference between gelatin/agar and gelatin was not significant), and gelatin/LA gellan gum was least stiff (3,615 ± 1,121 Pa, N = 4), although not significantly so.

Results from both methods of measuring fracture toughness place the gels in the same order of increasing toughness, and numbers were fairly similar between the two methods (Table 2). K-carrageenan/glucomannan is significantly tougher than the other gels, and from method 2, gelatin/agar is significantly tougher than gelatin/LA gellan gum. Gelatin/ι-carrageenan has similar fracture toughness to gelatin, gelatin/agar has a slightly higher toughness, and gelatin/LA gellan gum is slightly less tough. Method 1, using measured internal pressures of bubbles, resulted in fairly high r^2 for regressions for gelatin (r^2 = 0.69–1.00 for N = 4–16) and gelatin/ι-carrageenan (r^2 = 0.40–1.00 for N = 2–6), moderate r^2 for gelatin/agar (r^2 = 0.41– 0.59 for N = 5–8), and low r^2 for κ-carrageenan/glucomannan (r^2 = 0.08–0.29 for N = 2–5) and gelatin/LA gellan gum (r^2 = 0.06–0.41 for N = 2–6). The low r^2 for κ-carrageenan/glucomannan was unsurprising considering the problems with obtaining this measurement (discussed in methods). Method 1 was expected to underestimate K_{Ic}, whereas Method 2 was expected to overestimate K_{Ic}, and true K_{Ic} likely falls between the results from the two methods, 161.9 ± 37.3 Pa (mean ± S.D., N = 5) and 257.4 ± 9.1 Pa (N = 4), respectively. In the gelatin/LA gellan gum, the bubble sometimes grew down or to the side as well as growing upward in the aquarium, possibly because the fracture toughness was low, allowing the crack to extend easily. This variability may have contributed to the low r^2 in this material.

Stiffnesses and fracture toughnesses of gels were lower than measured E and K_{Ic} of natural sediments, but the ratios of K_{Ic}/E of the gels fall within the range for natural sediments (Fig. 5A). Stiffness and fracture toughness data for natural sediments are

Table 2. Mechanical properties of gels. Stiffnesses (E) and fracture toughnesses (K_{Ic}) of the five gels. Because polymer gels are notoriously temperature sensitive in their mechanical properties, all measurements were made in a temperature-controlled room at 11°C. Different lower-case letters (a, b, c) indicate significant differences among treatments from ANOVA results.

Material	Gelatin	Gelatin/ ι-carrageenan	Gelatin/ agar	κ-carrageenan/ glucomannan	Gelatin/LA gellan gum	ANOVA results
E (Pa)	$7100 \pm 372^{a,b}$ (N = 8)	6880 ± 1464^{a} (N = 5)	16855 ± 1672^{b} (N = 6)	8258 ± 1281^{a} (N = 5)	3615 ± 1121^{a} (N = 4)	$F(4,35) = 6.61$ $p = 0.0005$
K_{Ic} (Pa $m^{0.5}$) (Method 1)	58.1 ± 8.2^{a} (N = 3; $r^2 = 0.69$–1.00 for n = 4–16*)	58.7 ± 4.2^{a} (N = 3; $r^2 = 0.40$–1.00 for n = 2–6)	84.7 ± 5.5^{a} (N = 5; $r^2 = 0.41$–0.59 for n = 5–8)	161.9 ± 37.3^{b} (N = 5; $r^2 = 0.08$–0.29 for n = 2–5)	43.0 ± 2.3^{a} (N = 4; $r^2 = 0.06$–0.41 for n = 2–6)	$F(4,20) = 19.93$ $p < 10^{-6}$
K_{Ic} (Pa $m^{0.5}$) (Method 2)	$65.4 \pm 9.5^{a,b}$ (N = 3)	$69.4 \pm 2.4^{a,b}$ (N = 2)	112.1 ± 12.6^{a} (N = 4)	257.4 ± 9.1^{c} (N = 4)	35.5 ± 3.2^{b} (N = 3)	$F(4,20) = 37.65$ $p < 10^{-8}$
K_{Ic}/E ($m^{0.5}$) (Method 1)	0.0082 ± 0.0016	0.0085 ± 0.0024	0.0050 ± 0.0008	0.0196 ± 0.0076	0.0119 ± 0.0043	
K_{Ic}/E ($m^{0.5}$) (Method 2)	0.0092 ± 0.0018	0.0101 ± 0.0025	0.0067 ± 0.0014	0.0312 ± 0.0059	0.0098 ± 0.0039	

*N = number of gels tested, n = number of increments of bubble growth (i.e., points in regression).

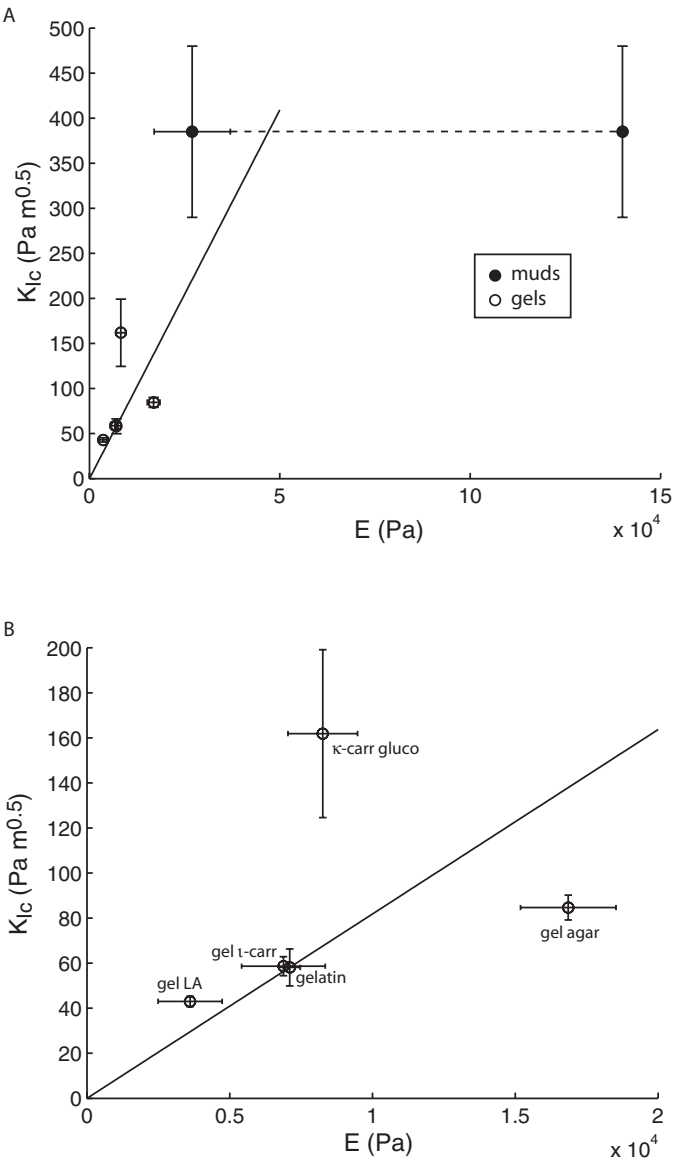

Figure 5. Fracture toughness (K_{Ic}) calculated with method 1 plotted against stiffness (E). Error bars indicate standard deviations. A line from the origin through the K_{Ic} of gelatin separates tougher (above) from stiffer (below) materials. A: Gels (open circles) are compared to natural muds (closed circles). Stiffnesses of natural muddy sediments were measured on the surface of sediments from Lowes Cove, ME (2.4×10^4 Pa; Dorgan *et al.,* 2007) and in subsurface sediments from Cole Harbour, Nova Scotia, Canada (1.4×10^5 Pa; Johnson *et al.,* 2002). The dashed line indicates stiffnesses at intermediate depths in the sediment, which likely fall between the two measured stiffnesses. Fracture toughness has been measured only in sediments from Cole Harbour (280 to 490 Pa m$^{0.5}$; Johnson *et al.,* 2002), and this range is indicated for both measured stiffnesses. B: Fracture toughness plotted against stiffness for only the gels used in this study (note different axes).

extremely limited; both properties have been measured in sediment cores from Cole Harbour, Nova Scotia, Canada (Johnson *et al.,* 2002; Boudreau *et al.,* 2005), and stiffness has also been measured in sediment cores from Lowes Cove, ME (Dorgan *et al.,* 2007). This limited sample size and geographic range clearly make extrapolation to all muddy sediments tenuous, but they are the only existing data. Among the gels, the ratio K_{Ic}/E is

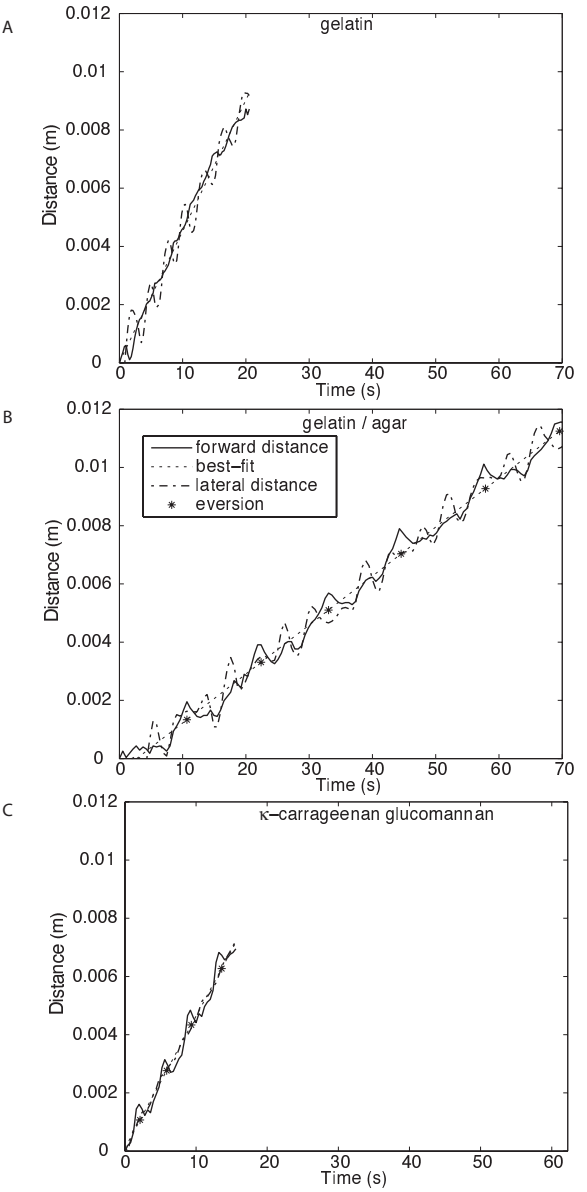

similar for gelatin, gelatin/ι-carrageenan, and gelatin/LA gellan gum (Fig. 5B). Gelatin/agar has a lower K_{Ic}/E and κ-carrageenan/glucomannan has a higher K_{Ic}/E than other gels.

c. Burrowing mechanics: Dorsal view analyses

Three different behaviors were observed in video segments in the five different gels (Fig. 6, Table 3). Most of the worms in gelatin and gelatin/LA gellan gum extended their burrows by moving their heads from side-to-side and did not evert their pharynges (Fig. 6A). In gelatin, one worm everted its pharynx once, but only the dorsal view was recorded and it was not included in the analysis of pharynx eversion behavior because there were not multiple eversions from which to calculate time and distance between eversions. In the gelatin/LA gellan gum gel, several worms everted their pharynges only once. One worm everted its pharynx multiple times, and that dorsal-view video was analyzed. Three of five worms in the gelatin/ι-carrageenan gel did not evert their pharynges, instead burrowing by moving their heads from side-to-side.

Most of the worms burrowing in gelatin/agar (3/4) everted their pharynges and moved their heads from side-to-side between pharynx eversions (Fig. 6B). Two out of five worms in gelatin/ι-carrageenan showed this behavioral pattern, as did one out of six worms burrowing in gelatin/LA gellan gum.

All of the worms burrowing in the κ-carrageenan/glucomannan gel everted their pharynges but did not move their heads from side-to-side to extend the burrow laterally (Fig. 6C). For conciseness, data on pharynx eversion behavior for these worms are presented in Table 3 with the worms that everted their pharynges and moved their heads, but the behaviors were clearly different.

Velocities, forward distances traveled per cycle, and periods of cycles were compared among gels for each behavioral category (except for pharynx eversion with no head movement, which occurred only in the toughest gel). Worms in gelatin moved faster, had shorter periods of head movement and moved forward farther with each cycle of head

←

Figure 6. Distance moved, recorded from dorsal-view video segments. The solid line is the forward distance taken from a best-fit line through the x-z coordinates of the anterior end of the worm. The dot-dash line is the lateral distance moved by the anterior end of the worm. Residuals were added to the best-fit line through the distance data (the slope of which is the worm's velocity) to superimpose the lateral head movement on the forward distance moved. Times of observed pharynx eversions (*) are plotted along the best-fit line. A: Representative worm burrowing in gelatin. The sinusoidal, lateral head movement can be seen clearly from the dotted line. The worm was moving straight ahead at a constant velocity, which is shown by the near linearity of the solid line of distance vs. time. There were no pharyngeal eversions. B, Representative worm burrowing in gelatin/agar by alternating pharynx eversions and head movements. The pharynx eversions are shown as peaks in the plot of forward distance. (Forward distance increases quickly when the pharynx is everted, then decreases when the pharynx is retracted.) Between pharyngeal eversions, the head moves from side-to-side, visible in the dotted, lateral distance plot. C, Representative worm burrowing in κ-carrageenan/ glucomannan. Again pharynx eversions are visible as peaks in the forward distance plot. The lateral distance plot is linear, lacking periodic head movements.

Table 3. Data from analysis of dorsal-view video. A: Worms with no pharynx eversions. B: Worms that everted pharynges. Normalized lateral distance of head movement was calculated from the full amplitude of the residuals from the best-fit, 2nd order polynomial (because the worm often moved in a curved path) through the *x*–*z* coordinates of the anterior end of the worm. The lateral distance of head movement was normalized by dividing by the width of the worm measured at the 4th setiger. The two categories of behavior in which the pharynx was everted were combined to make the table more concise. None of the worms burrowing in κ-carrageenan/glucomannan moved its head laterally, whereas all worms burrowing in other materials did. Different lower-case letters (a, b, c) indicate significant differences among treatments from ANOVA results.

Material	Gelatin	Gelatin/ ι-carrageenan	Gelatin/ agar	κ-carrageenan/ glucomannan	Gelatin/LA gellan gum	ANOVA results
Occurrence of side-to-side head movement	6/6	3/5	2/4*	0/6	5/6	
Normalized lateral distance (dimensionless)	0.59 ± 0.10	0.44 ± 0.24	0.78 ± 0.11		0.62 ± 0.30	F(3,12) = 0.97 p = 0.44
Period (s)	2.48 ± 0.43[a]	3.37 ± 0.37[a,b]	5.14 ± 1.45[b]		3.88 ± 0.85[b]	F(3,12) = 7.93 p = 0.0035
Velocity (mm/s)	0.55 ± 0.13[a]	0.26 ± 0.08[b]	0.15 ± 0.04[b]		0.25 ± 0.12[b]	F(3,12) = 11.04 p = 0.0009
Forward distance (mm/s)	1.31 ± 0.10[a]	0.88 ± 0.20[b]	0.75 ± 0.01[b]		0.90 ± 0.24[b]	F(3,12) = 8.58 p = 0.0026

*One worm exhibited side-to-side head movements in one video segment and periodic pharynx eversions in another video segment so was included in both analyses.

Table 3B.

Material	Gelatin	Gelatin/ ι-carrageenan	Gelatin/ agar	κ-carrageenan/ glucomannan	Gelatin/LA gellan gum	ANOVA results
Occurrence of pharynx eversions	0/6	2/5	3/4*	6/6	1/6	
Period of eversion cycle (s)		9.12 ± 3.13	9.31 ± 3.64	7.99 ± 3.69	7.6	F(3,8) = 0.16 p = 0.92
Forward distance (mm cycle^{-1})		1.45 ± 0.21	1.53 ± 0.67	1.44 ± 0.46	4.1**	F(2,8) = 0.87 p = 0.45
Velocity (mm s^{-1})		0.17 ± 0.08	0.15 ± 0.04	0.21 ± 0.07	0.54**	F(2,8) = 0.03 p = 0.97
Period of head movement between eversions (s)		3.20 ± 0.52	4.22 ± 0.75	N/A***	2.8	F(2,3) = 2.26 p = 0.25
Normalized lateral distance of head movement (dimensionless)		0.71 ± 0.05[a]	0.97 ± 0.04[b]	N/A***	0.66[a]	F(2,3) = 27.06 p = 0.012

*One worm exhibited side-to-side head movements in one video segment and periodic pharynx eversions in another video segment so was included in both analyses.

**Not included in ANOVA. Inclusion results in F(3,8) = 8.88, p = 0.0063 and F(3,8) = 10.06, p = 0.0043 for forward distance and velocity respectively.

***No worms in κ-carrageenan/glucomannan exhibited periodic head movement between pharynx eversions.

movement than worms in the other materials. Worms in gelatin/agar moved slightly slower with longer periods and shorter distances moved in each cycle, although the differences were not significant. There were no significant differences in the velocities and velocity components for worms that everted their pharynges. The one worm that everted its pharynx in gelatin/LA gellan gum moved forward farther in each cycle and consequently at a higher velocity than worms in other materials, but only one worm was observed in this material. We calculated ANOVAs both including and excluding this worm and found that inclusion of this datum resulted in significant differences among gels, whereas exclusion resulted in no significant differences (Table 3B).

Comparison of lateral head movement among gels indicated that worms in gelatin/agar moved their heads farther from side-to-side than worms in the other materials, both between pharynx eversions (significant difference) and when the pharynx was not everted (difference was not significant). The normalized lateral distance was calculated for comparison among worms that differed in size as the full amplitude of the head movement, measured in the center of the anterior tip of the worm, divided by the measured width of the 4th setiger of the preserved worm. Normalized lateral distance is dimensionless, whereas normalization of thicknesses uses average worm width for dimensions of length.

d. Burrowing mechanics: Lateral view analyses

Because video segments of both dorsal and lateral views were not obtained for all worms, some worms were included in both dorsal and lateral analyses and some were included in only one. The numbers of worms exhibiting each of the three behaviors in the lateral view video segments (Table 4) are therefore similar but not exactly the same as those for the dorsal view segments (Table 3).

Calculated K_I values from worm thicknesses for worms that did not evert their pharynges were very close to K_{Ic} values for each of the four materials (Table 4A). The normalized body thickness (multiplied by (average width of all worms measured)/(individual worm width)) of the worm in gelatin/agar was slightly lower than for worms in other materials, but as only one worm was included, it may not be a true difference. Sensitivity analyses showed that calculations of K_I and a are fairly robust to errors in measured worm width (presented in Appendix A).

Maximum K_I values for worms that everted their pharynges were higher than the K_{Ic} values for gelatin/agar, gelatin/ι-carrageenan, and gelatin/LA gellan gum, but were lower than K_{Ic} for κ-carrageenan/glucomannan (Table 4B). Changes in shapes of worms as the pharynx was everted and inverted were most apparent in gelatin/agar and least apparent in κ-carrageenan/glucomannan (shown in Fig. 7 for representative worms in each material; no worms everted their pharynges in gelatin, so this material was excluded). Real thicknesses were used to calculate K_I (Fig. 7A), but normalized thicknesses of both the body and the pharynx are presented for comparison among different gels (Fig. 7B). Average normalized body and pharynx thicknesses at the maximum K_I were higher in κ-carrageenan/glucomannan and lower in gelatin/agar (Table 4B, Fig. 7B). Body and pharynx thicknesses were smaller and showed greater variability across a pharynx eversion

Table 4. Data from analysis of lateral-view video. A: Worms with no pharynx eversion. B: Worms that everted their pharynges. Body half-thickness (h) and pharynx half-thickness were normalized by multiplying by the average width of worms measured at the 4th segment divided by the width of the individual worm. Different lower-case letters (a, b, c) indicate significant differences among treatments from ANOVA results.

Material	Gelatin	Gelatin/ ι-carrageenan	Gelatin/ agar	κ-carrageenan/ glucomannan	Gelatin/LA gellan gum	ANOVA results
Calculated K_I (Pa $m^{0.5}$)	57.6 ± 7.9	60.7 ± 5.2	116.4		34.7 ± 7.2	
K_{Ic} (Pa $m^{0.5}$)	58.1 ± 8.2*	58.7 ± 4.2*	84.7 ± 5.5* 112.1 ± 12.6**		43.0 ± 2.3* 35.5 ± 3.2**	
h, Normalized body half-thickness (mm)	0.75 ± 0.03	0.90 ± 0.17	0.68		0.80 ± 0.16	F(3,9) = 1.07 p = 0.41
$(a - b)$ (mm)	1.41 ± 0.22	2.09 ± 1.40	1.51		1.48 ± 0.33	F(3,9) = 0.63 p = 0.62
Slope at a	0.18 ± 0.05	0.19 ± 0.05	0.15		0.23 ± 0.06	F(3,9) = 1.01 p = 0.43
N	4	3	1	0	5	
t-test H_a: $K_I \neq K_{Ic}$	p = 0.94	p = 0.62			p = 0.06*, 0.86**	

*Calculated using method 1.
**Calculated using method 2.

Table 4B.

Material	Gelatin	Gelatin/ ι-carrageenan	Gelatin/ agar	κ-carrageenan/ glucomannan	Gelatin/LA gellan gum	ANOVA results
Maximum K_I (Pa $m^{0.5}$)		114.6 ± 14.5	195.7 ± 8.8	127.2 ± 10.1	64.6	
K_{Ic} (Pa $m^{0.5}$)		58.7 ± 4.2*	84.7 ± 5.5* 112.1 ± 12.6**	161.9 ± 37.3* 257.4 ± 9.1**	43.0 ± 2.3* 35.5 ± 3.2**	
h, Normalized body half-thickness (mm)		$0.825 \pm 0.148^{a,b}$	0.589 ± 0.065^{a}	0.904 ± 0.106^{b}	$0.754^{a,b}$	F(3,9) = 8.02 p = 0.0065
Normalized pharynx half-thickness (mm)		$0.892 \pm 0.036^{a,b}$	0.676 ± 0.078^{a}	0.916 ± 0.106^{b}	$0.914^{a,b}$	F(3,9) = 6.04 p = 0.016
$(a - b)$ (mm)		0.478 ± 0.085	0.623 ± 0.098	0.500 ± 0.067	0.508	F(3,9) = 2.35 p = 0.14
Slope at a		0.631 ± 0.060	0.461 ± 0.103	0.568 ± 0.064	0.493	F(3,9) = 2.62 p = 0.11
N	0	2	4	6	1	
t-test H_a: $K_I \neq K_{Ic}$		p = 0.0066*	p < 0.001***	p = 0.055* p < 0.001**	p = 0.0037* p = 0.015**	

*Calculated using method 1.
**Calculated using method 2.
***For both method 1 and 2.

cycle in gelatin/agar. Thicknesses were larger and showed less variability in κ-carrageenan/ glucomannan.

Distances from the anterior end of the worm to the dorsoventral contact with the crack

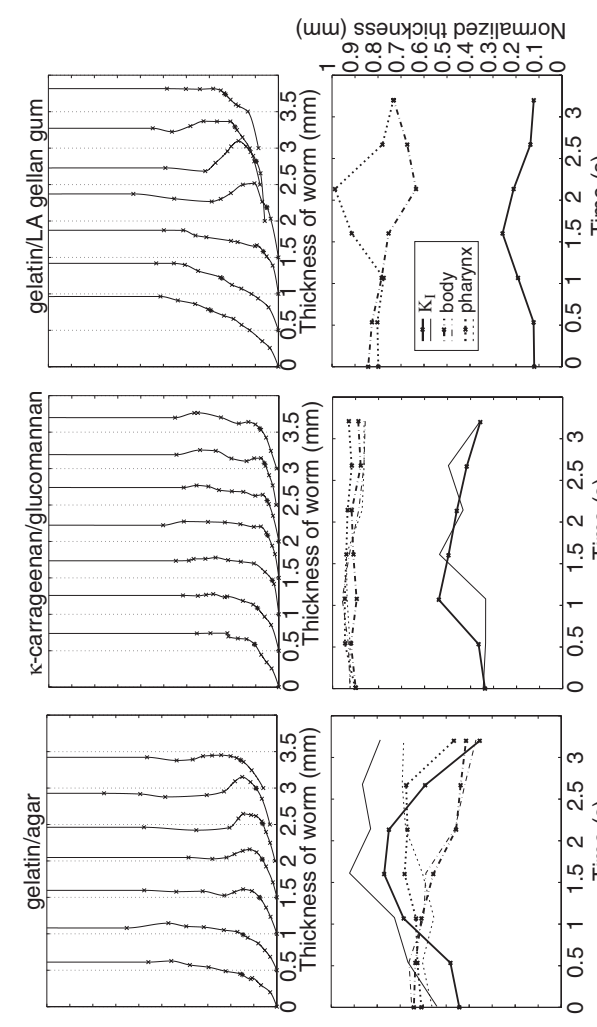

Figure 7. A: Worm thickness profiles over a cycle of pharynx eversion for representative worms in each material. The first profile is plotted with the crack tip at (0,0), and each subsequent profile is offset 0.5 mm farther to the right. When the anterior of the worm was at a distance $b > 0$ from the crack tip, the tip of the profile started at the distance b from the crack tip, which is always at the origin. Asterisks indicate points of contact of the worm with the crack wall, calculated from Eqs. 1 and 4, and x's are individual measurements of width from which profiles were interpolated. B: K_I (solid line), calculated from worm profiles shown in (A) are indicated with thick lines and x's. Normalized body half-thickness (h, dot-dash line) and pharynx half-thickness (dotted line) for the same worm are also indicated with thick lines and x's. Thin lines with no x's are calculated from a different worm in each material (other than gelatin/LA gellan gum, in which only one worm everted its pharynx), for which profiles are not shown. Pharynx half-thickness was calculated as the largest thickness between the crack tip at $y = 0.002$ m. Both thicknesses were normalized by multiplying by average worm width and dividing by the individual worm width (to obtain thickness in m).

wall ($a - b$), which were calculated simultaneously with K_I, did not differ significantly among gels, although they were slightly greater in the gelatin/agar gel. The point of contact was approximately 0.5 mm from the front of the worm, consistent with previous images of stress fields around worms, in which the compressive stress field around the pharynx begins approximately half way between the anterior end of the worm and the maximal thickness of the everted pharynx (cf. Dorgan *et al.,* 2007). The slope of the everted pharynx at the point of contact also did not differ significantly among gels.

4. Discussion

a. Differences in burrowing behavior

The three different behaviors exhibited by worms among the different gels can be explained by differences in mechanical properties of those gels. Side-to-side head movement reduces the effect of stiffness on the burrower by extending the crack edges away from the worm laterally. Worms in the stiffest (lowest K_{Ic}/E) material (gelatin/agar) moved their heads the greatest lateral distances, whereas worms in the toughest (highest K_{Ic}/E) material (κ-carrageenan/glucomannan) showed no head movement. Additionally, worms in the toughest material (κ-carrageenan/glucomannan) everted their pharynges and had thicker bodies than worms in other materials, as predicted.

Initially we were surprised that worms everted their pharynges in the stiff gelatin/agar, as we expected that pharynx eversion would be unnecessary to extend the crack. The stress intensity factor being close to the critical value for the one worm that did not evert its pharynx supports our prediction that the worms would not need to evert their pharynges to extend the crack, and indeed peak stress intensity factors greatly exceeded the critical values when the pharynx was everted. One possible explanation for this behavior is that the pharynx eversion extends the crack anteriorly to reduce the effect of stiffness on the anterior end of the worm. We have used finite element modeling to show that internal pressure needed to maintain body shape decreases as the crack edge is extended laterally away from the worm (cf. Dorgan *et al.,* 2007). It follows that anterior crack extension should reduce pressure in the head region. However, finite element modeling of anterior and lateral crack extension suggests that the reduction in internal pressure required to maintain body shape is not as important for anterior as for lateral crack extension (see Appendix B).

The high K_I relative to K_{Ic} during pharynx eversions in gelatin/agar, gelatin/ι-carrageenan, and gelatin/LA gellan gum implies that the crack extends anterior to the worm, which is difficult to see in the videos because the gelatin/agar (in which most pharynx eversions occurred) was somewhat translucent rather than completely transparent, and polarizers had been oriented to allow enough light to see the worm clearly. The crack is most easily visible when the polarizers are crossed, and becomes very difficult to see as the polarizers block less light. We had calculated K_I assuming that the crack extended only as far as the anterior end of the worm, as observed in previous experiments in gelatin (cf. Dorgan *et al.,* 2007). To calculate how far the crack would extend in front of the worm

(since $K_I > K_{Ic}$), the stress intensity factor was calculated for increasing distance between the wedge and the crack tip (b in Eq. (1)) until the stress intensity factor decreased to K_{Ic}. Calculated b for gelatin/agar is 1.3 ± 0.4 mm (mean ± S.D., N = 4), for gelatin/ι-carrageenan is 1.4 ± 0.3 (N = 2), and for gelatin/LA gellan gum is 1.2 (N = 1). These distances are very close to the forward distances moved by the worms in one pharynx eversion cycle (1.53 ± 0.67 (N = 3), 1.45 ± 0.21 (N = 2), and 4.1 (N = 1) mm respectively). These results suggest that pharynx eversion (rather than head movement) is the primary means of crack extension in these materials. We had predicted that pharynx eversion would not be necessary to extend the crack in stiffer materials, and this prediction was supported by K_I values close to K_{Ic} for worms not everting their pharynges. The mechanics show that pharynx eversion behavior in stiff materials extends the crack out in front of the worm, in contrast to our previous results suggesting that the crack tip extends with (and no farther than) the anterior end of the worm (Dorgan *et al.,* 2007). Both behaviors are supported by mechanics and the increased use of pharynx eversion in the stiffest material suggests that extending the crack anteriorly may be advantageous in maintaining body shape. Anterior crack extension may also accommodate feeding along the wall of the burrow.

In the toughest material, the κ-carrageenan/glucomannan gel, none of the worms showed periodic, side-to-side head movement. Unfortunately, this gel was the most opaque, and the shape of the burrow could not be resolved (nor could the shape of bubbles, as discussed in methods). The lack of head movement suggests that the lateral edges of the crack were much closer to the worm than in other gels. This assumption is supported by observed close proximity of the antennae to the worm's body compared to their postures in gelatin. In gelatin, in which the crack shape is clearly visible, antennae often trace anterior to lateral edges of the crack. This toughest gel was the only one in our experiment for which the calculated stress intensity factor did not exceed, or even reach, the critical value for the material. This result was initially surprising, as the worms were clearly extending their burrows and moving forward, and the criterion for crack extension is that K_I equals or exceeds K_{Ic}. However, use of the 2D wedge equation to calculate K_I is based on the 2D plane strain assumption that the displacements and stresses are constant across the width of the worm. We have previously suggested that the reason this 2D approximation works for burrowing worms is that side-to-side head movement removes the lateral constraint by extending the crack laterally (cf. Dorgan *et al.,* 2007). Because worms in the κ-carrageenan/glucomannan gel showed no lateral head movement, it follows that this assumption does not hold for this material. The results using the wedge equation do not make sense mechanically, likely because the assumptions of the wedge equation are invalid in this material. The close proximity of the lateral constraint would allow the worm to build up higher internal pressures and exert more stress (cf. Appendix B), leading to a higher stress intensity factor, potentially reaching or exceeding K_{Ic}, than calculated in the 2D problem. However, the importance of the 3rd dimension in this case makes the problem much more complicated, and calculation of an accurate stress intensity factor would require 3D, finite element modeling.

In the tough κ-carrageenan/glucomannan gel, all worms exhibited the same behavior, whereas in the very stiff gelatin/agar gel, most but not all of the worms exhibited behavior characteristic of high stiffness. This difference may simply result from our choice of gels; the κ-carrageenan/glucomannan may be more extreme and therefore worms exhibit more consistent behaviors. Additionally, our sample sizes are too small to make conclusive statements about several of the behavioral differences. It seems plausible, however, that toughness would be a greater constraining factor on behavior than stiffness. Mechanically, if K_I does not exceed K_{Ic}, the crack will not grow. An increase in stiffness requires an increase in internal pressure to maintain body shape. Maintaining a higher internal pressure requires the worm to expend more energy, but only when the worm reaches its physiological maximum strength does a discrete change in its ability to move occur (assuming that there is a discrete physiological maximum strength). It follows that the greater the differences in burrowing energetics between the two behaviors observed in gelatin/agar, the sharper the transition between the two behaviors. Forces exerted by *Nereis virens* during pharynx eversion increase directly with sediment stiffness (Dorgan *et al.,* 2007). Smaller forces are required to deform a material smaller distances, so the forces exerted by *Nereis virens* burrowing by moving its head from side-to-side should be lower than during pharynx eversion. These smaller forces are exerted over smaller distances, but for longer periods, so external work done may be similar. Research on burrowing energetics in different materials may help to explain these different behaviors.

Differences in behavior of worms in gelatin and in gelatin/ι-carrageenan were observed, however, even though neither stiffness nor fracture toughness differed significantly between the two materials. Addition of ι-carrageenan was expected to make the gel tougher and less stiff, and although the means followed the trend expected, differences were small and not statistically significant, in part because of the large variability in stiffness of the gelatin/ι-carrageenan. Because this gel set very quickly, variability in mechanical properties between replicates and spatial heterogeneity within replicates may have resulted from small differences in the time between boiling and pouring into the aquaria. Although we tried to measure fracture toughness and stiffness for each aquarium used, initial attempts to measure stiffness by applying a weight to the surface of the gel and measuring displacement with a camera resulted in high variability (because camera-measured displacements were not precise enough). More precise stiffnesses were measured near the end of the experiments using the Vitrodyne tester. In addition, about half of our attempts to measure fracture toughness failed due to bubble leaking or contact of the bubble with the bottom of the tank (resulting from initiating too large a bubble). Without data on fracture toughness and stiffness for each aquarium and with small sample sizes, it is impossible to determine whether the differences in behaviors between gelatin and gelatin/ι-carrageenan and within gelatin/ι-carrageenan are statistically significant and if so result from variability in material properties.

Worms varied considerably in time to start burrowing, during which the worm either moved very little or repeatedly backed out of the initial crack. These differences in behavior were difficult to quantify (and are not shown), in part because the behavior

depended on how often the worm was re-inserted into the crack and poked with the pipet. Although velocity data were collected and are presented for each material (Table 3), the velocity likely depended on how much energy was expended by the worm before starting to burrow, which differed among worms and was not quantified. Higher velocities of worms in gelatin and the one worm that everted its pharynx in gelatin/LA gellan gum may reflect lower fatigue levels due to greater 'willingness' to burrow in these materials.

The three different behaviors appear to be used in three different mechanical regimes. The head movement without pharynx eversions seen in gelatin may represent a response to material of intermediate toughness and stiffness. Pharynx eversions with large side-to-side head movements may be characteristic of stiff materials, and pharynx eversions without head movements may characterize tough materials. These different behaviors suggest the need for a dimensionless number to characterize the material in which burrowing occurs.

b. Dimensionless "wedge" number

Components of external work for a worm to move forward in its burrow a distance Δx include work to extend the crack by fracture a distance Δx, work to deform the elastic material enough to make room for the worm's body, inertial work, and work done against friction. The energy of fracture, W_{Cr} (J), is

$$W_{Cr} = G_c(\Delta x)w_{crack} \tag{9}$$

where G_c is the crack resistance (or critical energy release rate) (energy L^{-2}), Δx is the distance that the crack extends (L), and w_{crack} is the width of the crack (L). Fracture occurs when the available energy for fracture, G, exceeds G_c, the amount of energy released when the crack grows and a unit area of new crack is formed. This energy-based fracture criterion is more convenient in calculating work of fracture than is the stress intensity factor, K_I, as a criterion of fracture, and in plane strain, G is related to K_I through stiffness and Poisson's ratio as

$$G = \frac{K_I^2(1 - \nu^2)}{E} \text{ (Anderson, 1995).} \tag{10}$$

The work, W_{el} (energy), to deform an elastic material with stiffness E (force L^{-2}) in order to move forward Δx follows a proportionality rule given by

$$W_{El} \propto Ehw_{worm}(\Delta x) \tag{11}$$

where h is the thickness of the worm (L), and w_{worm} is the width of the worm (L). Inertial work can be ignored because burrowers move slowly (cf. Alexander, 2003).

Friction can be ignored in this first-order approximation because frictional work is roughly proportional to the work to deform the elastic material (the elastic restoring force is the normal force, which is multiplied by a friction coefficient to obtain the friction force). The frictional work would be added to the elastic work to obtain the work to move forward, so assuming the friction coefficient and worm size to be constant, including the frictional

work would have the same effect as multiplying the elastic work by a constant. In addition, we have suggested that work against friction may be less significant than previously thought because worms move by peristaltic waves in which stationary, dilated segments withstand most of the elastic restoring force, enabling narrower, extended segments to move against relatively small frictional forces (Dorgan *et al.,* 2006).

The work to burrow a unit distance is therefore the sum of the work of fracture (Eq. (9)) and the elastic work (Eq. (11)),

$$\frac{W_{tot}}{\Delta x} = \frac{W_{Cr} + W_{El}}{\Delta x} = G_c w_{crack} + Ehw_{worm}. \tag{12}$$

The ratio of these components of external work can be expressed as a dimensionless "wedge" number, *Wg*,

$$Wg = \frac{G_c}{Eh}\frac{w_{crack}}{w_{worm}}. \tag{13}$$

The dimensionless wedge number is the ratio of the work of fracture to the work against the elastic restoring force of the sediment and scales with the square of the ratio of K_{Ic} to E, as related through Eq. (10),

$$\frac{G_c}{Eh}\frac{w_{crack}}{w_{worm}} = \left(\frac{K_{Ic}}{E}\right)^2 \frac{(1-\nu^2)}{h}\frac{w_{crack}}{w_{worm}}. \tag{14}$$

If the wedge number is large, burrowing is essentially a fracture problem; if it is small, maintaining body shape should be a bigger problem than propagating the crack.

Observations of worms burrowing in gels with differing K_{Ic}/E (or G_c/E) show that worms exhibit behaviors that reduce a high wedge number or increase a low wedge number. The thickness of the worm (h) normalized to worm width varies as a function of (G_c/E). If G_c/E is small, the worm moves its head from side-to-side to increase the width of the crack relative to the width of the worm, increasing the second part of the wedge number. If G_c/E is large, the worm thickness is relatively large and the width of the crack does not extend much beyond the width of the worm (Fig. 8). Side-to-side motion of the head has been noted in previous burrowing studies (e.g., Elder, 1973; Hunter *et al.,* 1983); here we posit one function for such motion and suggest its likely relation to material properties. Like many behaviors developed through natural selection, it likely increases fitness through multiple effects, possibly enhancing chemosensory abilities as well as maintaining body shape.

Both E and K_{Ic} are higher in natural sediments than in these gels, although the ratios of K_{Ic}/E for the gels fall within the range of those for natural sediments (cf. Fig. 5). We observed obvious behavioral differences in gels with a smaller range of K_{Ic}/E values than those in natural sediments. The range of K_{Ic}/E values in natural sediments, as well as the absolute values of both K_{Ic} and E, is poorly understood. The rigid particles in natural sediments are expected to increase their stiffness, but may also cause stress softening (Koehl, 1982), reducing the effect of stiffness on burrowers over time. Higher fracture

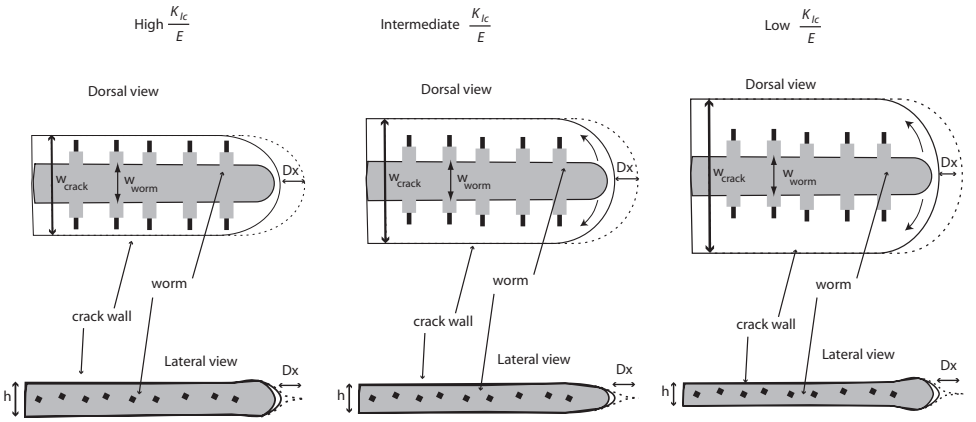

Figure 8. Scheme of differences in burrowing mechanics with wedge number. Worm width is indicated at the 4th setiger.

toughness in natural sediments than gels might result from microcracking around particles. Clearly, more research on the mechanical properties of muds on spatial and temporal scales relevant to burrowers is needed to predict burrowing behaviors in natural sediments. Conversely, observations in transparent gels containing particles of the same refractive index would also clearly be worthwhile in an attempt to match mechanics of the simplified media to those of natural sediments.

Pharyngeal eversions are used for both burrowing and feeding; understanding how behavior depends on sediment mechanics may also lend insight into subsurface feeding behaviors. We showed that worms in the stiffer gels could effectively extend the burrow either by pharynx eversion or by driving the head forward in the crack. None of the worms were feeding while burrowing in the gels, effectively separating burrowing behavior from feeding behavior in our experiments. In natural sediments, worms may be feeding while everting their pharynges to extend the crack or may feed from the crack walls without extending the crack. Understanding burrowing mechanics can help identify when and at what frequency pharynx eversions are necessary for crack extension.

In natural sediments, these differences in behavior likely affect particle movements differently and therefore have implications for bioturbation. Particle mixing likely depends on the width of the crack, which varies with the ratio of fracture toughness to stiffness. In materials with high stiffness, side-to-side motion may be a major driver of bioturbation during burrowing. These different behaviors may also be more or less effective in creating a permanent burrow after crack extension by fracture; intuitively, larger forces exerted during pharynx eversion and repeated application of forces through changes in body thickness would be more effective at deforming sediments plastically. In materials with high fracture toughness, the large forces needed to produce a crack may be sufficient to rearrange particles plastically at the crack tip. In order to predict how movement of sediment grains varies with worm behavior, more research on sediment mechanics is

needed, specifically on whether and how sediment grains are released from the matrix under forces exerted by burrowers. Once these interactions are known, stratigraphic effects can be predicted through automaton modeling (e.g., Choi *et al.,* 2002; Reed *et al.,* 2006).

We also emphasize that behaviors differ among species, with potentially large consequences for bioturbation. We have suggested that the mechanism of burrowing by crack propagation is widespread (Dorgan *et al.,* 2006), and it seems likely that mechanical properties would affect burrowing behavior in burrowers of other taxa as well. Variations of burrowing behavior and their consequences across a broad spectrum of animal sizes and species merit attention.

The differences in nereidid behavior with sediment properties observed also support making further investigations into whether and, if so, how these burrowing-relevant mechanical properties of sediments depend on classically measured factors such as grain size, porosity and quantity and quality of organic material. If they do not, then new mechanical measurements need to be added to the arsenal in order to understand the strong feedbacks in organism-sediment interactions. Because bulk sediment behaves so much like an elastic polymer, it is clear that the polymeric matrix that binds muddy sediments warrants greater attention from both mechanical and chemical perspectives.

5. Conclusions

Worms burrowing in gels with different mechanical properties exhibited variations in body shapes and behaviors that were predicted from fracture mechanics theory. Behaviors depend on the ratio of fracture toughness to stiffness, and a dimensionless "wedge" number was developed to compare work done by the worms against the stiffness of muds to maintain body shape and that to extend a burrow by fracture. Few data exist on stiffness and fracture toughness in natural sediments, but the range of K_{Ic}/E values in muds likely is close to or exceeds that of the gels used, suggesting that these behavioral differences occur in natural sediments and supporting the need for further research on the mechanical properties of muds.

Acknowledgments. This research was funded by an NSF Graduate Research Fellowship and an NDSEG Fellowship to K. Dorgan and by ONR Grant N00014-03-1-0776 to P. A. Jumars. The authors would like to thank Bob Lad and Eric Martin at the University of Maine Laboratory for Surface Science and Technology (LASST) for use of the Vitrodyne Tester. We also thank FMC Biopolymer for providing complimentary samples of carrageenans. In addition, we thank Eric Landis, Bernard P. Boudreau and Larry M. Mayer for valuable comments during the research and on earlier drafts and two anonymous reviewers for helpful comments on the manuscript.

APPENDIX A

Sensitivity of wedge-driven stress intensity factor to worm thickness measurement

The stress intensity factor K_I generated by a worm in a burrow in an elastic solid is given as a function of the following parameters if the problem is treated as one of wedge-driven fracture. The distance from the crack tip to the head of the worm is b, the distance from the

crack tip to the point at which the burrow wall contacts the worm body is a, with $a > b$, and the worm profile is given by $\pm f(x - b)$, where x is the distance from the crack tip. The material parameters of the problem are the elastic modulus E and the Poisson's ratio ν. The stress intensity factor can thus be schematically denoted by

$$K_I(b, a, f(x - b), E, \nu).$$

All parameters of the problem are observed and measured except for the distance a. This lack of observational data requires simultaneous solution of two equations for the unknowns K_I and a. The key observations necessary to calculate K_I measure the worm profile $\pm f(x - b)$. In this study the worm profile is measured at 10 points. The addition of an initial value of $f_0 = 0$ and a remote value $f_1 = h$ brings the total number of parameters defining the worm profile to 12, of which 11 are free, since $f_0 = 0$ is a requirement for compatible geometry. Denoting the free observations of the worm profile by f_i, $i = 1{:}11$, the stress intensity factor can be denoted

$$K_I(b, a, f_1, f_2, \ldots, f_{11}, E, \nu).$$

The sensitivity of the stress intensity to the worm profile measurements is

$$D_i = \frac{dK_I}{df_i}, \quad i = 1, 2, \ldots, 11.$$

These sensitivities are useful in understanding how observational error or uncertainty affects the calculated stress intensities. Since we do not have an analytic form of the stress intensity factor for this problem, we approximate the derivative shown above by a finite difference

$$D_i = \frac{K_I(f_i + \delta f_i) - K_I(f_i - \delta f_i)}{2\delta f_i}$$

where δf_i is a small but finite perturbation to the worm profile observation. If we set $\delta f_i = 0.05 f_i$, so that we use a 5 percent perturbation on the observed worm profile, we obtain sensitivities D_i with magnitudes ranging between 0.2×10^4 and 10×10^4 Pa $m^{-1/2}$, with a mean magnitude of 1.5×10^4 Pa $m^{-1/2}$.

The images from which the worm profiles are observed have a scaling factor of 0.0113 m/pixel. Therefore, an error of 2 pixels (one on each end of the measured line) in reading the worm profile results in an error between 0.08 Pa $m^{1/2}$ and 4.4 Pa $m^{1/2}$ in the computed stress intensity factor. These errors are small relative to the magnitude of stress intensity factors computed for typical worms.

The sensitivity of a can also be computed using a finite difference approach as described above if we treat a as a function of f_i. Again using a perturbation of 5 percent of f_i, sensitivities range between 0.05×10^3 and 3.3×10^3 mm m^{-1}, which correspond to errors in a of 2.2×10^{-3} mm and 1.5×10^{-1} mm for a two-pixel error in observation of f_i. These errors are also small.

Our conclusion is that the solution for K_I and a is robust to mild error in the observation

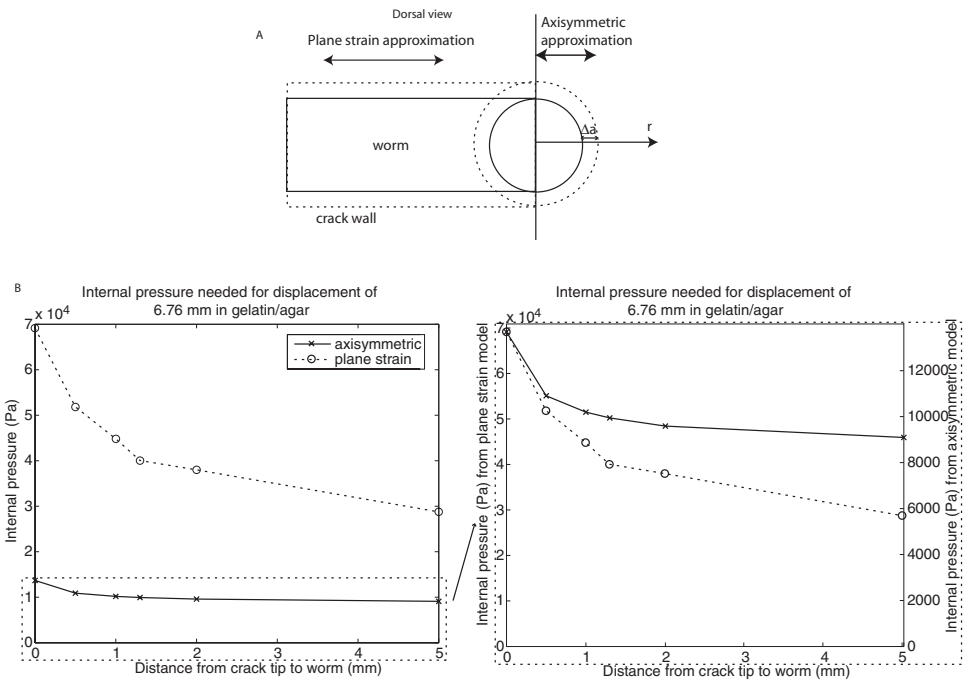

Figure 9. Internal pressure required for the worm to maintain constant body shape (or displacement) as the crack extends away from the worm. A: A 2D plane strain model represents the lateral crack extension away from the body of the worm, and a 2D axisymmetric model represents the anterior crack extension. B: Internal pressure required for the worm to maintain constant body shape decreases as the crack extends away from the worm in both the plane strain and axisymmetric models. In the plane strain model, the effect of extending the crack away from the worm is greater than in the axisymmetric model. The plane strain model underestimates the decrease in pressure as the crack extends because it does not include the wedging effect in the 3rd dimension (cf. Dorgan *et al.,* 2007). The axisymmetric model overestimates the decrease in pressure because it is more constrained than the anterior of the worm, which is constrained axially only 180° anterior of the worm rather than the whole 360° in the model, resulting in overestimation of pressure, the effect of which decreases as the crack extends away from the worm. We therefore expect that the reduction of internal pressure required to maintain body shape is even more substantial in the lateral (plane strain model) direction than the anterior (axisymmetric model) direction than predicted by the models.

of the worm profile. The situation is ameliorated further by the argument that the errors in reading the worm profile would not be systematic, and so will tend to cancel each other out.

APPENDIX B

Effect of anterior crack extension on internal pressure

We calculated the effect of anterior crack extension on pressure using a 2D, axisymmetric, finite element model and compared results to those from lateral crack extension modeled in 2D plane strain (Fig. 9). Neither model is a good approximation of the worm,

although comparison of model results with consideration of the assumptions of the two models does provide useful information. We showed that the 2D anterior view, plane strain model with measured stresses applied to the crack walls does not accurately predict body thickness of nereidids and suggested that removal of the lateral constraint allows the worm to use its body as a wedge to pry apart the sediment (Dorgan *et al.,* 2007). This deduction implies that when the lateral crack edge is very close to the worm, the model more accurately predicts displacements, and as the lateral crack edge extends away from the worm, modeled displacements will increasingly underestimate actual displacements. In other words, the internal pressure needed to maintain body shape as predicted by the model will be most accurate for small distances between the worm's body and the crack tip and will overestimate pressures as the crack extends away from the worm. This difference in error would lead to underestimation of the decrease in required pressure shown in Figure 9B. It suggests that the benefit of extending the lateral crack edge in stiff materials is even greater than predicted by the model (Fig. 9B). In contrast, the axisymmetric model likely overestimates pressures for small distances between the crack tip and the worm and is comparable to the true pressure or more accurate as the distance between the crack tip and the worm increases. In other words, the benefit of extending the anterior crack edge is less than predicted by the model (Fig. 9B). The axisymmetric model is more constrained than the 3D worm because the axisymmetric model assumes that the anterior constraint applies 360° around the worm's head rather than the actual 180°. Greater constraint results in larger stresses to maintain a given displacement. As the crack extends, the constraint is removed, and the deviation of the model either does not change or decreases. This line of reasoning suggests that although anterior crack extension does decrease the internal pressure required to maintain body shape, and therefore may be beneficial in stiff materials, the effect is not as great as for lateral crack extension.

REFERENCES

Alexander, R. M. 2003. Principles of Animal Locomotion, Princeton University Press, Princeton, NJ, 365 pp.

Anderson, T. L. 1995. Fracture Mechanics: Fundamentals and Applications. CRC Press, Boca Raton, FL, 680 pp.

Barenblatt, G. I. 1962. The mathematical theory of equilibrium cracks in brittle fracture, *in* Advances in Applied Mechanics v. 7, H. L. Dryden and T. von Karman, eds., Academic Press, 55–129.

Boudreau, B. P., C. Algar, B. D. Johnson, I. Croudace, A. Reed, Y. Furukawa, K. M. Dorgan, P. A. Jumars, A. S. Grader and B. S. Gardiner. 2005. Bubble growth and rise in soft sediments. Geol., *33,* 517–520.

Choi, J., F. Francois-Carcaillet and B. P. Boudreau. 2002. Lattice-automaton bioturbation simulator (LABS): implementation for small deposit feeders. Computers and Geosciences, *28,* 213–22.

Dorgan, K. M., S. R. Arwade and P. A. Jumars. 2007. Burrowing in marine muds by crack propagation: kinematics and forces. J. Exp. Biol., *210,* 4198–4212.

Dorgan, K. M., P. A. Jumars, B. D. Johnson and B. P. Boudreau. 2006. Macrofaunal burrowing: the medium is the message. Ocean. Mar. Biol., *44,* 85–141.

Dorgan, K. M., P. A. Jumars, B. D. Johnson, B. P. Boudreau and E. Landis. 2005. Burrow elongation by crack propagation. Nature, *433,* 475.

Elder, H. Y. 1973. Direct peristaltic progression and the functional significance of the dermal

connective tissues during burrowing in the polychaete *Polyphysia crassa* (Oersted). J. Exp. Biol., *58,* 637–55.

Fett, T. 1982. Crack opening displacement of a penny-shaped crack in an infinite body loaded by internal pressure over a circular area. Int. J. Fracture, *20,* R135–R138.

Gray, J. S. 1974. Animal-sediment relationships. Ocean. Mar. Biol., *12,* 223–261.

Hunter, R. D. and H. Y. Elder. 1989. Burrowing dynamics and energy cost of transport in the soft-bodied marine invertebrates *Polyphysia crassa* and *Priapulus caudatus.* J. Zool., *218,* 209–222.

Hunter, R. D., V. A. Moss and H. Y. Elder. 1983. Image analysis of the burrowing mechanisms of *Polyphysia crassa* (Annelida: Polychaeta) and *Priapulus caudatus* (Priapulida). J. Zool., *199,* 305–23.

Johnson, B. D., B. P. Boudreau, B. S. Gardiner and R. Maass. 2002. Mechanical response of sediments to bubble growth. Mar. Geol., *187,* 347–363.

Jumars, P. A., K. M. Dorgan, L. M. Mayer, B. P. Boudreau and B. D. Johnson. 2007. Physical constraints on infaunal lifestyles: May the persistent and strong forces be with you, *in* Trace Fossils: Concepts, Problems, Prospects, W. Miller, III, ed., Elsevier, Amsterdam, 442–457.

Koehl, M. A. R. 1982. Mechanical design of spicule-reinforced connective tissue: Stiffness. J. Exp. Biol., *98,* 239–267.

Mach, K. J., D. V. Nelson and M. W. Denny. 2007. Techniques for predicting the lifetimes of wave-swept macroalgae: a primer on fracture mechanics and crack growth. J. Exp. Biol., *210,* 2213–2230.

Meysman, F. J. R., J. J. Middelburg and C. H. R. Heip. 2006. Bioturbation: a fresh look at Darwin's last idea. Trends Ecol. Evol., *21,* 688–695.

Phillips, G. and P. Williams. 2000. Handbook of Hydrocolloids. Woodhead Publishing, Cambridge, England, 472 pp.

Ramey, P. A. and P. V. R. Snelgrove. 2003. Spatial patterns in sedimentary macrofaunal communities on the south coast of Newfoundland in relation to surface oceanography and sediment characteristics. Mar. Ecol. Prog. Ser., *262,* 215–227.

Reed, D. C., K. Huang, B. P. Boudreau and F. J. R. Meysman. 2006. Steady-state tracer dynamics in a lattice-automaton model of bioturbation. Geochim. Cosmochim. Acta, *70,* 5855–5867.

Sih, G. C. 1973. Handbook of stress intensity factors: Stress intensity factor solutions and formulas for reference. Lehigh University, Bethlehem, PA.

Timoshenko S. P. and J. N. Goodier. 1970. Theory of Elasticity, McGraw-Hill, NY, 608 pp.

Received: *29 November, 2007;* revised: *16 April, 2008.*